Novel Auxiliary RISE (ARISE) Robust Control Approaches for Nonsmooth or Switched Nonlinear Systems

by

Sujata Basyal

A thesis submitted to the Graduate Faculty of
Auburn University
in partial fulfillment of the
requirements for the Degree of
Master of Science

Auburn, Alabama
August 3, 2024

Keywords: ARISE Controller, Signum function, Sliding Mode Controller

Approved by

Brendon Allen, Chair, Assistant Professor of Mechanical Engineering
Dan Marghitu, Professor of Mechanical Engineering
Chad Rose, Assistant Professor of Mechanical Engineering

Abstract

To deal with uncertainties in a dynamic system, many nonlinear control approaches have been considered. Unique challenges arise from uncertainties that are bounded by constants, which led to the development of both continuous and discontinuous control methods. One such approach that yields a favorable transient performance is sliding mode (SM) control. However, SM control requires rapid switching within the control input due to a discontinuous signum function in the control architecture, which introduces chattering during real-world application. To address the limitations of SM control while still exploiting its advantages and robustness, a class of continuous robust controllers named Robust Integral of the Sign of the Error (RISE) was developed. RISE controllers include an integral of the signum function, not a signum function, in the control law. Filtering the signum function with an integral makes the signum function continuous and thereby mitigates chatter that would result from a discontinuous SM term. Even though RISE controllers exhibit a significant level of robustness, it is limited to classes of smooth nonlinear dynamic models.

In the first part of this thesis, a novel auxiliary RISE (ARISE) controller is proposed to prevent chattering and deal with uncertainties (even those bounded by constants) for general, switched, and nonsmooth control-affine nonlinear systems. The ARISE control system includes a unique auxiliary error that is designed to inject a discontinuous SM term directly into the error system without including a SM term in the controller itself akin to the RISE control architecture. Consequently, the ARISE control law minimizes the chattering effect that results from discontinuous SM terms. The proposed ARISE control system is augmented with an adaptive update law to deal with the unknown control effectiveness matrix in the dynamic model. To prove the effectiveness of the ARISE controller, a nonlinear stability analysis was conducted and resulted in semi-global exponential tracking towards an

ultimate bound. Furthermore, the performance of the proposed controller was evaluated and compared against a traditional SM controller through simulations using a switched Van der Pol oscillator model. The simulations were conducted in Matlab/Simulink, and the results of the comparisons are shown in various graphs. It is concluded that the proposed ARISE controller performs better for a switched system than the SM controller. The improved performance of the ARISE controller was consistent across different dynamic parameters and disturbances.

In the second part of this thesis, the ARISE controller is modified to account for the physical limitations of actuators. Specifically, to enhance the applicability of the ARISE control approach, a saturated hyperbolic tangent function is incorporated into the control input to allow the controller to be bounded a priori, which will account for the limitations of physical actuators during real-world applications. A nonsmooth Lyapunov-like stability analysis is performed for the proposed saturated ARISE control system to prove that the closed-loop error system is uniformly ultimately bounded for a switched dynamic model. A series of numerical simulations were performed to compare the performance of the saturated ARISE controller with a standard saturated SM controller across different dynamic parameters and disturbances.

In Chapter 1 of this thesis, the motivation to develop an ARISE controller is described. After that, the dynamic model for general, nonsmooth, and control-affine systems is presented in Chapter 2. The control-affine dynamic model is modified to be switched to validate the proposed ARISE controller's ability to be implemented in switched and nonsmooth systems. In Chapter 3, the control development, stability analysis, and simulations on a switched dynamic model are provided for the ARISE controller. The effectiveness of the developed ARISE controller is analyzed and compared with a standard SM controller across varying dynamic parameters by conducting a series of simulations. In Chapter 4, the development of a saturated ARISE controller, its stability analysis, and its simulations on a switched system are presented. A simulation analysis similar to the ARISE controller is completed for the saturated ARISE controller. Finally, in Chapter 5, the thesis is concluded by summarizing the contribution of each chapter and discussing future efforts.

Acknowledgments

I would like to extend my heartfelt gratitude to my advisor, Dr. Brendon Allen, for his invaluable advice, support, and encouragement throughout this project. Working under Dr. Allen has been a great learning experience, not only in acquiring technical skills but also in developing the ability to think critically and see beyond the obvious. I am deeply grateful for his patience and consideration throughout my research, as well as for his kind and helpful support.

I am thankful for Dr. Dan Marghitu and Dr. Chad Rose serving on my thesis committee. I am grateful for their valuable recommendations and insights.

I am grateful to my colleagues in the CARE Lab for encouraging me during my graduate studies. My deepest appreciation goes to my family, whose love and support were instrumental in accomplishing this project. I am appreciative of my friends for their consistent support throughout my career.

Table of Contents

List of Figures

List of Tables

List of Abbreviations

SM	Sliding Mode
RISE	Robust Integral of the Sign of Error
ARISE	Auxiliary RISE
RMS	Root Mean Square

Chapter 1

Introduction

1.1 Background

Over many years, research has been ongoing in the field of control design for complicated, uncertain nonlinear dynamic systems [1, 2, 3, 4, 5, 6, 7, 8, 9]. Given that most real-world systems exhibit nonlinear behavior, nonlinear control design is a topic of practical significance [10]. Due to the robustness and adaptability of nonlinear controllers, they are often preferred over linear control approaches for nonlinear systems [11, 12]. To get the best stability outcomes in the presence of system uncertainty and nonlinearities, various nonlinear control approaches have been developed by numerous researchers [13, 14, 15, 16]. For example, a high-gain control is a common robust control approach that is used to deal with model uncertainty [17]. However, the robust high-gain controllers do not provide the best control and error convergence results when uncertain or unstructured terms within the dynamics can only be upper bounded by constants. To enhance the performance of the controller and obtain a better stability outcome, robust controllers have been combined with feedforward adaptive terms to compensate for the uncertain parameters [18, 19, 20, 21]. To elaborate, adaptive terms in a control law are capable of reducing the amount of control effort needed for the system to converge since some of the uncertainty has been isolated and approximated by feedforward terms. Thus, a feedforward adaptive term incorporates some dynamic information in the control law, thereby enhancing controller performance.

Another approach to compensate for dynamic uncertainties that are bounded by constants is to augment robust or adaptive controllers with discontinuous terms. For example, sliding mode (SM) controllers incorporate a discontinuous signum function within the control law to compensate for these uncertain terms [15, 22, 23, 24]. Theoretically, SM is a robust control approach that immensely enhances stability and yields a favorable transient performance despite the system uncertainties being upper bounded by a constant; however, the discontinuous signum function within the SM controller architecture introduces abrupt switching within the control input [25]. Though SM controllers are known for their robustness to uncertainties, this rapid switching between differing control actions requires infinite control frequency and introduces chattering, all of which hinder the practical application of SM control [18, 26, 27, 28]. Chattering is a high-frequency oscillation that can lead to undesirable effects like noise, and wear and tear in mechanical systems, thereby reducing control accuracy while operating in real-world dynamic systems [29].

To harness the benefits and minimize the drawbacks of SM control, researchers have investigated ways to reduce SM-induced chatter [30, 31, 32]. Various method has been investigated to reduce chatter caused by discontinuous SM function [30, 31, 32, 33]. Most notably, Robust Integral of the Sign of the Error (RISE) controllers have been used over SM control due to their ability to eliminate chatter [18, 32, 34, 35, 36, 37, 38, 39, 40]. RISE control, which is a high-gain feedback control approach, was developed to address the shortcomings of SM control while still exploiting its advantages and robustness. Unlike conventional SM control development methods where a signum function is included directly in the control input, the signum function is instead included in the time derivative of an auxiliary error system in the RISE-based approach. Incorporating the auxiliary error in the RISE control input introduces an integral SM term in the control law, rather than a SM term itself, making the control input continuous. The continuous RISE controller eliminates the SM controller's requirement for infinite control frequency and reduces chattering, bolstering the RISE controller's utility in real-world systems.Unlike SM control, RISE control is a class of continuous robust controllers that includes an integral of the signum function instead of the signum function itself in the control law. Specifically, the RISE control approach filters the discontinuous signum function through an integrator, yielding a continuous output, thereby mitigating chatter. Beyond mitigating chatter, RISE controllers attain excellent stability results both theoretically and in practice for uncertain dynamic systems. In fact, the RISE control structure is highly capable of compensating for additive disturbances and model uncertainties within the system dynamics with finite control gains [39, 41, 42, 43]. Moreover, the RISE-based approach can be both modular and model-independent, depending upon the system objectives. In terms of stability, RISE controllers typically produce an asymptotic convergence of the tracking errors, provided that the dynamic model obeys an underlying assumption that the system dynamics and disturbances are sufficiently smooth and possess bounded time derivatives [32, 34, 35, 36, 38, 39, 40, 44, 45, 46]. RISE-based control systems have also demonstrated exponential convergence of the error system after some modifications in the control structure and stability analysis [47]. Previously developed RISE-based approaches have not only been used to control a dynamic system [37, 44, 48, 49], but they have also been used for a variety of other applications; for example, RISE-based approaches have been used for system estimation [39, 50, 51], delay compensation [32, 52], and system optimization [53]. In terms of practical applications, RISE controllers have excelled in controlling a wide range of real-world dynamic systems. These systems include, but are not limited to, autonomous underwater vehicles, autonomous aerial vehicles, delayed systems, and rehabilitative robotics [18, 39, 54, 55, 56].

1.2 Motivation

The RISE control method is a robust control approach that accounts for additive system disturbances and parametric uncertainties, and is derived under the assumption that the time derivative of the dynamic model is continuously differentiable. Though RISE controllers are highly robust and leverage the benefits of SM controllers all while mitigating their downsides, the requirement of the dynamic model being differentiable limits the applicability of RISE approaches to continuous and smooth systems. Furthermore, the requirement that the dynamic model is differentiable also requires the control inputs to be differentiable, which precludes the application of RISE methods in switched/discontinuous systems. These shortcomings of the RISE controller brings forth an open question, *can a chatter-mitigating feedback control structure be developed for a wide class of uncertain nonlinear systems, including switched or nonsmooth systems, to compensate for unknown terms in the open-loop error system that are upper bounded by constants?* This thesis answers this motivating question by developing a novel ARISE controller for general, nonsmooth, and switched dynamic systems.

1.3 Outline of the Thesis

In Chapter 2, a nonlinear, switched, and control-affine dynamic model for the development of the ARISE controller is presented.

In Chapter 3, the development of the first ARISE controller, its stability analysis, and its performance analysis through numerical simulations are presented. The ARISE controller is designed to account for the shortcomings of RISE controllers while still exploiting its advantages. The control architecture of the ARISE controller includes an integral of the signum function, similar to the RISE control architecture, and is implementable in a wide range of uncertain nonlinear systems including switched/discontinuous systems. Similar to RISE control, the SM term is introduced indirectly into an open-loop error system to compensate for uncertainties and to eliminate chatter that results from the direct injection of a discontinuous SM term in the control structure. To inject the SM term into the open-loop error system, a filtered error signal is developed. Even though the closed-loop error system has the SM term, the controller itself includes an integral SM term, which reduces the need for an infinite control frequency, thereby mitigating chattering. The control effectiveness used in the dynamics in this thesis is considered to be unknown and potentially switched or nonsmooth. To account for the uncertain control effectiveness matrix, an adaptive estimate is proposed. A nonsmooth Lyapunov-like stability analysis is performed to confirm the efficacy of the proposed adaptive ARISE control system. The stability result shows that the proposed control system results in semi-global exponential trajectory tracking towards an ultimate bound. A series of numerical simulations are performed using a modified two-state Van der Pol oscillator as the dynamic model to validate the performance of the proposed control system. The performance of the ARISE controller was compared with a traditional SM controller to determine their relative effectiveness. The root mean square (RMS) errors were calculated for the trajectory tracking errors for both controllers across varying dynamic parameters and disturbances to evaluate both approaches' robustness. The comparison results demonstrated that the ARISE controller is more robust than the SM controller.

Chapter 4, building upon the work in Chapter 3, implements a smooth hyperbolic tangent function as a saturation function in the control structure to enable the ARISE controller to be bounded a priori while still ensuring system stability and convergence. It is necessary to saturate the control structure to guarantee that the control input does not exceed the physical limitations of the actuator(s). If the control effort is more than the limitations of real-world actuators, there may be undesired mechanical and thermal issues, which can hinder the application of the control system. In Chapter 4, the development and analysis of the saturated ARISE control approach is presented.

In Chapter 5, the overall conclusions of the thesis are provided. This chapter incorporates a summary of each chapter with their respective contribution. The potential directions for future work are also included in this chapter.

Chapter 2

Dynamic Model

In this chapter, the dynamic model of a general, nonsmooth, uncertain, and control-affine nonlinear system is considered. The dynamic model used for the controller development is

$$\dot{x}(t) = f_{\sigma}(x(t)) + d_{\sigma}(t) + \underbrace{g_{\phi}(x(t), t)\, u(t)}_{\tau_{\phi}(x(t),t)}, \tag{2.1}$$

where $x : \mathbb{R}_{\geq 0} \to \mathbb{R}^n$ represents the generalized states, $f_{\sigma} : \mathbb{R}^n \to \mathbb{R}^n$ represents the uncertain, nonlinear, and nonsmooth drift dynamics, and $d_{\sigma} : \mathbb{R}_{\geq 0} \to \mathbb{R}^n$ represents the nonsmooth and unknown disturbances. The signal $\sigma(x(t), t)$, denoted by $\sigma : \mathbb{R}^n \times \mathbb{R}_{\geq 0} \to \mathcal{P} \triangleq \{1, 2, \ldots, p\}$, represents an uncertain switching signal that indicates the index of $f_{\sigma}(x(t))$ and $d_{\sigma}(t)$, where the number of unique forms for $f_{\sigma}(x(t))$ and $d_{\sigma}(t)$ are represented by $p \in \mathbb{N}$. The generalized input torque or force in (2.1) is represented as $\tau_{\phi} : \mathbb{R}^n \times \mathbb{R}_{\geq 0} \to \mathbb{R}^n$ and is defined as the product of the control input $u : \mathbb{R}_{\geq 0} \to \mathbb{R}^m$ and the unknown and nonsmooth control effectiveness matrix $g_{\phi} : \mathbb{R}^n \times \mathbb{R}_{\geq 0} \to \mathbb{R}^{n \times m}$ as

$$\tau_{\phi}(x(t), t) = g_{\phi}(x(t), t)\, u(t). \tag{2.2}$$

The signal $\phi(x(t), t)$, denoted by $\phi : \mathbb{R}^n \times \mathbb{R}_{\geq 0} \to \mathcal{S} \triangleq \{1, 2, \ldots, s\}$, represents a known switching signal that indicates the index of $\tau_{\phi}(x(t), t)$ and $g_{\phi}(x(t), t)$, where the number of unique forms for $\tau_{\phi}(x(t), t)$ and $g_{\phi}(x(t))$ are represented by $s \in \mathbb{N}$.

Remark 2.1. Every unique form of $f_{\sigma}(x(t))$ and $d_{\sigma}(t)$ are represented by the signal $\sigma \in \mathcal{P}$, which switches values whenever $f_{\sigma}(x(t))$ and $d_{\sigma}(t)$ have a discrete jump. Likewise, every unique form of $\tau_\phi(x(t),t)$ and $g_\phi(x(t),t)$ are represented by the signal $\phi \in \mathcal{S}$, which switches values whenever $\tau_\phi(x(t),t)$ and $g_\phi(x(t),t)$ have a discrete jump. Whenever $\sigma \in \mathcal{P}$ and $\phi \in \mathcal{S}$ are constant, the dynamics in (2.1) are continuous (i.e. $f_\sigma(x(t))$, $d_\sigma(t)$, $g_\phi(x(t),t)$, and $\tau_\phi(x(t),t)$ are continuous for constant σ and ϕ).

The following assumptions must be satisfied to facilitate the control development:

Assumption 2.1. *The drift function $f_\sigma(x(t))$ is upper bounded by a known constant $c_F \in \mathbb{R}_{>0}$ such that $\|f_\sigma(x(t))\| \leq c_F$, $\forall t \geq t_0$ and $\forall \sigma \in \mathcal{P}$ whenever $\|x(t)\| \in \mathcal{L}_\infty$, where the term $t_0 \in \mathbb{R}_{\geq 0}$ represents the initial time and $\|\cdot\|$ represents the standard Euclidean norm.*

Assumption 2.2. *The disturbance $d_\sigma(t)$ is upper bounded by a known constant $c_D \in \mathbb{R}_{>0}$ such that $\|d_\sigma(t)\| \leq c_D$, $\forall t \geq t_0$ and $\forall \sigma \in \mathcal{P}$.*

Assumption 2.3. *The control effectiveness matrix $g_\phi(x(t),t)$ is a full-row rank matrix for all $t \geq t_0$.*

Assumption 2.4. *The generalized torque/force input $\tau_\phi(x(t),t) = g_\phi(x(t),t)\,u(t)$ can be linearly parameterized for all $t \geq t_0$ such that*

$$g_\phi(x(t),t)\,u(t) = Y_\phi(x(t),t,u(t))\,\theta, \tag{2.3}$$

where $\theta \in \mathbb{R}^q$ represents a vector of the unknown constants in $g_\phi(x(t),t)$ and $q \in \mathbb{N}$ represents the number of uncertain constants in $g_\phi(x(t),t)$. The matrix $Y_\phi : \mathbb{R}^n \times \mathbb{R}_{\geq 0} \times \mathbb{R}^m \to \mathbb{R}^{n \times q}$ represents a measurable regression matrix. Also, the portions of $g_\phi(x(t),t)$ that vary explicitly with time are assumed to be bounded such that $g_\phi(x(t),t) \in \mathcal{L}_\infty$ whenever $x(t) \in \mathcal{L}_\infty, \forall t \geq t_0$. The i^{th} parameter in θ, denoted by θ_i, can be upper and lower bounded by $\bar{\theta}_i \in \mathbb{R}$ and $\underline{\theta}_i \in \mathbb{R}$, respectively, such that $\theta \in \mathcal{L}_\infty$ and

$$\underline{\theta}_i \leq \theta_i \leq \bar{\theta}_i, \forall i \in \{1,\ldots,q\}. \tag{2.4}$$

Remark 2.2. The control torque $\tau_{\phi}(x(t),t)$ in (2.1) is defined in such a way that it enables switching between multiple control inputs. It is defined as

$$\tau_{\phi}(x(t),t) \triangleq \sum_{i\in\mathcal{U}} g_i(x(t),t)\, u_i(x(t),t), \tag{2.5}$$

where $g_i : \mathbb{R}^n \times \mathbb{R}_{\geq 0} \to \mathbb{R}^{n\times m}$ represents the uncertain i^{th} control effectiveness matrix, $u_i : \mathbb{R}^n \times \mathbb{R}_{\geq 0} \to \mathbb{R}^m$ represents the i^{th} control input, and $\mathcal{U} \triangleq \{1, 2, \ldots, l\}$, $l \in \mathbb{N}$ represents the number of control inputs. The i^{th} control input $u_i : \mathbb{R}^n \times \mathbb{R}_{\geq 0} \to \mathbb{R}^m$ can be defined as

$$u_i(x(t),t) \triangleq \gamma_i \phi_i(x(t),t)\, u(t), \tag{2.6}$$

where $u(t)$ represents the control input in (2.1), $\phi_i : \mathbb{R}^n \times \mathbb{R}_{\geq 0} \to \{0, 1\}$ represents a known piecewise right-continuous switching signal indicating i^{th} control input is active, and $\gamma_i \in \mathbb{R}_{>0}$ represents a known selectable constant corresponding to $i \in \mathcal{U}$. Furthermore, defining the unknown control effectiveness matrix in terms of i^{th} control effectiveness matrix as

$$g_{\phi}(x(t),t) \triangleq \sum_{i\in\mathcal{L}} g_i(x(t),t)\, \gamma_i \phi_i(x(t),t). \tag{2.7}$$

Using (2.7) in (2.5) yields $\tau_{\phi}(x(t),t) = g_{\phi}(x(t),t)\, u(t)$, which is same definition in (2.1). Note that $g_{\phi}(x(t),t)$ in (2.7) represents a lumped control effectiveness matrix. Additionally, the known switching signal $\phi_i(x(t),t)$ must be designed such that $g_{\phi}(x(t),t)$ is full-row rank at all times to satisfy Assumption 2.3 for all $i \in \mathcal{U}$ to ensure that control authority is maintained. [1]

[1] If $\phi_i(x(t),t)$ is designed to be a discontinuous switching signal then the i^{th} control input will be discontinuous, which has the downside of assuming infinite bandwidth. However, chatter can be mitigated through proper design of the switching signals (i.e., ensuring a small amount of time passes between each jump). If continuous control inputs are desired, then $\phi_i(x(t),t), \forall i \in \mathcal{U}$ can be designed to be continuous. Note that if $\phi_i(x(t),t)$ and $g_i(x(t),t)$ are continuous $\forall i \in \mathcal{U}$, then $g_{\phi}(x(t),t)$ is continuous and the index ϕ is a constant.

Chapter 3

ARISE controller

In this chapter, the development of the ARISE controller is explained in detail. The motivation for developing the ARISE controller was to answer an open question: *Can a chatter-mitigating feedback control structure be developed for a wide class of uncertain nonlinear systems, including switched or nonsmooth systems, to compensate for unknown terms in the open-loop error system that are upper bounded by constants?* This chapter presents the development of the first ever ARISE control architecture, which is a control approach that can compensate for unknown disturbances and uncertainties in a nonsmooth, uncertain, and control affine nonlinear dynamic system. In this chapter, first, a tracking error is defined followed by the development of an auxiliary filtered error that can inject a SM term indirectly into the closed-loop error system. The auxiliary error law is designed in such a way that the controller itself includes an integral SM term, not the SM term itself. The integral SM term in the controller compensates for unknown disturbances while mitigating chattering and reducing the need for an infinite control frequency. An adaptive estimate of the control effectiveness matrix is proposed since the control effectiveness used in the dynamics in (2.1) is considered to be unknown. Furthermore, a nonsmooth Lyapunov-like stability analysis is performed to confirm the efficacy of the proposed adaptive ARISE control system. The stability results show that, if the gain requirements are satisfied, the designed control system produces semi-global exponential trajectory tracking towards an ultimate bound. Additionally, a series of numerical simulations are carried out using a modified two-state Van der Pol oscillator as the dynamic model to validate the performance of the proposed control system. The oscillator was specifically modified by including control-affine control inputs and by enabling the model parameters to be switched. The performance of the proposed ARISE controller was compared with a traditional SM controller to determine their relative performances when implemented on a switched system. The root mean square (RMS) error was calculated for the trajectory tracking errors for both the ARISE and the SM controller across different disturbances and dynamic parameters to compare both approaches robustness. The comparison results demonstrated that the RMS tracking errors of the ARISE controller were less than that of the SM controller across every tested scenario, which indicates that the ARISE controller is more robust than the SM controller for the controlled switched system.

3.1 Control Development

The control objective in this work is to ensure that the generalized states in the dynamics in (2.1) track a sufficiently smooth desired trajectory denoted by $x_d : \mathbb{R}_{\geq 0} \to \mathbb{R}^n$. The desired trajectory x_d and its time derivative $\dot{x}_d$ are known and bounded such that $x_d, \dot{x}_d \in \mathcal{L}_\infty$. A known tracking error, denoted as $e : \mathbb{R}_{\geq 0} \to \mathbb{R}^n$, is defined as

$$e\left(t\right) \triangleq x\left(t\right) - x_d\left(t\right). \tag{3.1}$$

Another objective of this work is to modify the error system to inject a SM term into the open-loop error system (i.e., the SM term is not in the controller). This task is accomplished through the design of an auxiliary tracking error, denoted by $r : \mathbb{R}_{\geq 0} \to \mathbb{R}^n$, that is defined as

$$r\left(t\right) \triangleq e\left(t\right) + \alpha e_f\left(t\right), \tag{3.2}$$

where $e_f : \mathbb{R}_{\geq 0} \to \mathbb{R}^n$ represents an auxiliary filtered error signal and $\alpha \in \mathbb{R}_{>0}$ represents a user-defined control gain. The time derivative of the auxiliary filtered error is defined as

$$\dot{e}_f(t) \triangleq -k_1 \operatorname{sgn}(r(t)) - k_2 r(t) - \beta e_f(t), \tag{3.3}$$

where $k_1, k_2, \beta \in \mathbb{R}_{>0}$ are user-defined control gains and $\operatorname{sgn}(\cdot)$ represents the signum function. Notice that the filter dynamics in (3.3) can be solved to determine $e_f(t)$.

Taking the time derivative of (3.2) and using (2.1), (3.1), and (3.3) yields

$$\dot{r}(t) = f_\sigma(x(t)) + d_\sigma(t) + g_\phi(x(t), t)\, u(t) - \dot{x}_d(t) - \alpha k_1 \operatorname{sgn}(r(t)) - \alpha k_2 r(t) - \alpha\beta e_f(t). \tag{3.4}$$

For notational brevity, an auxiliary term $\chi_\sigma : \mathbb{R}_{\geq 0} \to \mathbb{R}^n$ is defined as

$$\chi_\sigma(t) \triangleq f_\sigma(x(t)) + d_\sigma(t). \tag{3.5}$$

The auxiliary term can be upper bounded using Assumptions 2.1 and 2.2 and Equations (3.1) and (3.2) such that

$$\|\chi_\sigma(t)\| \leq \Phi + \rho(\|z(t)\|)\, \|z(t)\|, \tag{3.6}$$

where $\rho(\cdot) : \mathbb{R} \to \mathbb{R}_{>0}$ is a known, radially unbounded, and strictly increasing positive function, $\Phi \in \mathbb{R}_{>0}$ is a known constant, and $z : \mathbb{R}_{\geq 0} \to \mathbb{R}^{2n}$ is a composite error vector defined as

$$z(t) \triangleq \begin{bmatrix} r^T(t) & e_f^T(t) \end{bmatrix}^T. \tag{3.7}$$

Substituting (3.5) into (3.4) yields an open-loop error function as

$$\dot{r}(t) = \chi_\sigma(t) + g_\phi(x(t), t)\, u(t) - \dot{x}_d(t) - \alpha k_1 \operatorname{sgn}(r_1(t)) - \alpha k_2 r(t) - \alpha\beta e_f(t). \tag{3.8}$$

Since the control effectiveness matrix $g_\phi(x(t), t)$ is unknown, the matrix must be estimated using an adaptive approach. In this work, the estimate of the generalized torque/force input is expressed as

$$\hat{g}_\phi(x(t), t)\, u(t) = Y_\phi(x(t), t, u(t))\, \hat{\theta}(t), \tag{3.9}$$

where $\hat{g}_\phi : \mathbb{R}^n \times \mathbb{R}_{\geq 0} \to \mathbb{R}^{n\times m}$ is an estimate of $g_\phi(x(t), t)$ and $\hat{\theta} : \mathbb{R}_{\geq 0} \to \mathbb{R}^q$ is an estimate of the unknown vector of constants θ. The difference between the uncertain parameters and their estimates results in a parameter estimation error, denoted as $\tilde{\theta} : \mathbb{R}_{\geq 0} \to \mathbb{R}^q$, that is defined as

$$\tilde{\theta}(t) \triangleq \theta - \hat{\theta}(t). \tag{3.10}$$

Assumption 3.1. *The estimate of the control effectiveness matrix $\hat{g}_\phi(x(t), t)$, $\forall t \geq t_0$ is a full-row rank matrix. The right pseudo inverse of $\hat{g}_\phi(x(t), t)$ is denoted as $\hat{g}_\phi^+ : \mathbb{R}^n \times \mathbb{R}_{\geq 0} \to \mathbb{R}^{m\times n}$, where $\hat{g}_\phi^+(\cdot) \triangleq \hat{g}_\phi^T(\cdot)\left(\hat{g}_\phi(\cdot)\,\hat{g}_\phi^T(\cdot)\right)^{-1}$. Also, $\hat{g}_\phi(x(t), t)$ is bounded such that $\hat{g}_\phi(x(t), t) \in \mathcal{L}_\infty$ provided that $\hat{\theta}(t)$ and $x(t)$ are bounded $\left(i.e.\ \hat{\theta}(t),\ x(t) \in \mathcal{L}_\infty\right)$.*

Adding and subtracting $Y(x(t), t, u(t))\,\hat{\theta}(t)$ in (3.8) and using (2.3), (3.9), and (3.10) yields a modified open-loop error system as

$$\begin{aligned} \dot{r}_1(t) &= \chi_\sigma(t) + Y_\phi(x(t), t, u(t))\,\tilde{\theta}(t) + \hat{g}_\phi(x(t), t)\,u(t) \\ &\quad -\dot{x}_d(t) - \alpha k_1 \mathrm{sgn}(r(t)) - \alpha k_2 r(t) - \alpha\beta e_f(t). \end{aligned} \tag{3.11}$$

Based on the open-loop error dynamics in (3.11), the control input is designed as

$$u(t) \triangleq \hat{g}_\phi^+(x(t), t)\left(-k_3 r(t) + (k_2 + \alpha\beta)\, e_f(t) + \dot{x}_d(t)\right), \tag{3.12}$$

where $k_3 \in \mathbb{R}_{>0}$ is a user-defined control gain. Similarly, the parameter estimate law is designed as

$$\dot{\hat{\theta}}(t) \triangleq \mathrm{Proj}\left(\Gamma_1 Y_\phi^T(x(t), t, u(t))\, r_1(t)\right), \tag{3.13}$$

where $\Gamma \in \mathbb{R}^{q\times q}$ is a positive definite, diagonal gain matrix and $\text{Proj}(\cdot)$ denotes the smooth projection algorithm defined in [57], which ensures that the estimate $\hat{\theta}(t)$ stays within bounds defined in (2.4) for $\theta(t)$. The controller from (3.12) is substituted into the open-loop error system in (3.11) to obtain a closed-loop error system as

$$\dot{r}_1(t) = Y_\phi(x(t), t, u(t))\tilde{\theta}(t) - (k_3 + \alpha k_2) r(t) - \alpha k_1 \text{sgn}(r(t)) + k_2 e_f(t) + \chi_\sigma(t). \tag{3.14}$$

The closed-loop error system in (3.14) has a SM term due to the implementation of the auxiliary error term e_f. The SM term compensates for uncertain terms upper bounded by constants in the dynamics. Due to the controller implementing the integral of the signum function, chattering is effectively reduced.

3.2 Stability Analysis

The i^{th} time when ϕ switches to $w \in \mathcal{S}$ can be represented by $\{t_i^{w,\text{on}}\}$, $\forall i \in \mathbb{N}$ and the i^{th} time when ϕ switches from $w \in \mathcal{S}$ can be represented by $\left\{t_i^{w,\text{off}}\right\}$, $\forall i \in \mathbb{N}$. Let $V_L : \mathcal{D} \times \mathbb{R}_{\geq 0} \to \mathbb{R}_{\geq 0}$, be a positive definite common Lyapunov-like candidate function that is continuously differentiable in y, where y is a concatenated state vector that is defined as

$$y \triangleq \begin{bmatrix} z^T & \tilde{\theta}^T \end{bmatrix}^T. \tag{3.15}$$

The Lyapunov candidate function V_L is defined within the domain $\mathcal{D} \subseteq \mathbb{R}^{2n+q}$ as[1]

$$V_L(y,t) \triangleq \frac{1}{2} r^T r + \frac{1}{2} e_f^T e_f + \frac{1}{2}\tilde{\theta}^T \Gamma^{-1}\tilde{\theta}, \tag{3.16}$$

where $\mathcal{D} \triangleq \{y \in \mathbb{R}^{2n+q} \,|\, \|y\| \leq \gamma\}$, $\gamma \in \mathbb{R}_{>0}$ is a known constant that satisfies the inequality[2] $\gamma \leq \inf\left\{\rho^{-1}\left(\left(\sqrt{2\alpha k_2 \delta}, \infty\right)\right)\right\}$, $\delta \in \mathbb{R}$ is a known constant defined as $\delta \triangleq \min\left(k_3,\ \beta - \frac{\varepsilon k_1}{2}\right)$,

[1]For notational brevity, all functional dependencies are hereafter suppressed unless required for clarity of exposition.

[2]For a set B, the inverse image is defined as $\rho^{-1}(B) \triangleq \{a \mid \rho(a) \in B\}$.

and $\varepsilon \in \mathbb{R}_{>0}$ is a selectable constant. Using the concatenated state vector y defined in (3.15), the Lyapunov-like function V_L can be upper and lower bounded as

$$\lambda_1 \|y\|^2 \leq V_L \leq \lambda_2 \|y\|^2, \tag{3.17}$$

where the constants $\lambda_1, \lambda_2 \in \mathbb{R}_{\geq 0}$ are defined as $\lambda_1 \triangleq \min\left(\frac{1}{2}, \frac{1}{2}\lambda_{\min}\left\{\Gamma^{-1}\right\}\right)$ and $\lambda_2 \triangleq \max\left(\frac{1}{2}, \frac{1}{2}\lambda_{\max}\left\{\Gamma^{-1}\right\}\right)$, $\lambda_{\min}$ is defined as minimum eigen value of $\{\cdot\}$, and $\lambda_{\max}$ is defined as the maximum eigen value of $\{\cdot\}$. Additionally, based on Assumption 2.4 and (3.15), V_L can further bounded as

$$\frac{1}{2}\|z\|^2 \leq V_1 \leq \frac{1}{2}\|z\|^2 + v_1. \tag{3.18}$$

In (3.18), the function $v_1 : \mathbb{R}^q \to \mathbb{R}_{\geq 0}$ is defined as

$$v_1 \triangleq \frac{1}{2}\lambda_{\max}\left\{\Gamma^{-1}\right\}\left\|\tilde{\theta}\right\|_{\max}^2, \tag{3.19}$$

where $\left\|\tilde{\theta}\right\|_{\max} \in \mathbb{R}_{>0}$ is the maximum value of $\left\|\tilde{\theta}(t)\right\|$ such that $\left\|\tilde{\theta}(t)\right\| \leq \left\|\tilde{\theta}\right\|_{max}, \forall t \geq t_0$, resulting from the projection algorithm in (3.13) and the bounds defined in Assumption 2.4. Moreover, let $\mathcal{S}_{\mathcal{D}} \subseteq \mathbb{R}^{2n+q}$ be a set of allowable initial conditions that maintain system stability, defined as

$$\mathcal{S}_{\mathcal{D}} \triangleq \left\{ y \in \mathbb{R}^{2n+q} \,\middle|\, \|y\| \leq \sqrt{\frac{\lambda_1}{\lambda_2}}\gamma \right\}. \tag{3.20}$$

Theorem 3.1. *Consider the uncertain, nonsmooth, and nonlinear dynamics in* (2.1) *that satisfies all assumptions defined in Chapters 2 and 3. The control input in* (3.12) *and the parameter update law in* (3.13) *ensure a semi-global exponential trajectory tracking to an ultimate bound in the sense that*

$$\|y(t)\|^2 \;\leq\; \tfrac{\lambda_2}{\lambda_1}\|y(t_0)\|^2 \exp\left(-\delta(t-t_0)\right) + \tfrac{v}{\lambda_1\delta}\left(1 - \exp\left(-\delta(t-t_0)\right)\right), \tag{3.21}$$

for all $t \in [t_0, \infty)$*, provided that* $y(t_0) \in \mathcal{S}_{\mathcal{D}}$*, where* $v \triangleq \delta v_1 + \frac{nk_1}{2\varepsilon}$*, and provided that the following gain conditions are satisfied:*

$$\beta > \frac{\varepsilon k_1}{2}, \quad \alpha k_1 \geq \Phi, \quad \sqrt{\frac{v}{\lambda_1 \delta}} \leq \gamma. \tag{3.22}$$

Proof. Since the closed-loop error system in (3.14) contain discontinuous terms, the time-derivative of (3.16) exists almost everywhere (a.e.) for all $t \in [t_0, \infty)$. Let $y(t)$ be a Filippov solution to the differential inclusion $\dot{y} \in K[h](y)$ for all $t \in [t_0, \infty)$, where $K[\cdot]$ is defined in [58] and $h : \mathbb{R}^{2n+q} \to \mathbb{R}^{2n+q}$ is defined as $h(y) \triangleq \begin{bmatrix} \dot{r}^T, & \dot{e}_f^T, & \dot{\tilde{\theta}}^T \end{bmatrix}^T$.

Consider times when $\phi = w$ for any arbitrary $w \in \mathcal{S}$ (i.e., $t \in \left[t_i^{w,\text{on}}, t_i^{w,\text{off}}\right)$ for some $i \in \mathbb{N}$). During these times the dynamic functions Y_ϕ, g_ϕ, and $\hat{g}_\phi$ are continuous; thus, $K[\hat{g}_\phi] = \hat{g}_\phi$ and $K[Y_\phi] = Y_\phi$. Taking the generalized time derivative of (3.16), using the calculus of $K[.]$ from [59], and using (3.3), (3.10), (3.13), and (3.14) yields

$$\begin{aligned} \dot{\tilde{V}}_L \subseteq\ & r^T \left(K[\chi_\sigma] + Y_\phi \tilde{\theta} - (k_3 + \alpha k_2) r - \alpha k_1 K[\text{sgn}(r)] + k_2 e_f \right) \\ & + e_f^T \left(-k_1 K[\text{sgn}(r)] - k_2 r - \beta e_f \right) - \tilde{\theta}^T \Gamma^{-1} \left(\Gamma Y_\phi^T r \right). \end{aligned} \tag{3.23}$$

Implementing (3.6) and (3.22) into (3.23), applying Young's Inequality, completing the squares, canceling common terms, and using the facts that $\dot{V}_L(y) \overset{\text{a.e.}}{\in} \dot{\tilde{V}}_L(y)$, $\|K[\text{sgn}(r)]\| \leq \sqrt{n}$, and $\|y\| \geq \|z\|$ yields

$$\dot{V}_L \overset{\text{a.e.}}{\leq} -k_3 \|r\|^2 - \left(\beta - \tfrac{\varepsilon k_1}{2}\right) \|e_f\|^2 + \tfrac{1}{4\alpha k_2} \rho^2(\|y\|) \|z\|^2 + \tfrac{nk_1}{2\varepsilon}. \tag{3.24}$$

Additionally, using (3.7), (3.18), $v \triangleq \delta v_1 + \frac{nk_1}{2\varepsilon}$, and $\delta \triangleq \min\left(k_3,\ \beta - \frac{\varepsilon k_1}{2}\right)$ with (3.24) yields the following bound

$$\dot{V}_L \overset{\text{a.e.}}{\leq} -\delta V_L + v, \tag{3.25}$$

$\forall t \in \left[t_i^{w,\text{on}}, t_i^{w,\text{off}}\right)$ provided that $y(t) \in \mathcal{D}$, $\forall t \in \left[t_i^{w,\text{on}}, t_i^{w,\text{off}}\right)$. Since $\dot{V}_L$ is bounded for any arbitrary $\phi \in \mathcal{S}$, it can likewise be bounded for all $\phi \in \mathcal{S}$. Hence, (3.16) is a common

Lyapunov-like function across all $t \in [t_0, \infty)$, which means that (3.25) holds true for all $t \in [t_0, \infty)$, provided that $y(t) \in \mathcal{D}$, $\forall t \in [t_0, \infty)$. The differential equation in (3.25) can be further solved to yield

$$V_L(t) \leq \left(V_1(t_0) - \frac{v}{\delta}\right) \exp\left(-\delta(t - t_0)\right) + \frac{v}{\delta}, \tag{3.26}$$

$\forall t \in [t_0, \infty)$, provided that $y(t) \in \mathcal{D}$, $\forall t \in [t_0, \infty)$. The solution in (3.21) in Theorem 3.1 can be determined using (3.17) and (3.26). Provided that $y(t_0)$ lies within $\mathcal{S}_D$ and the gain condition $\sqrt{\frac{v}{\lambda_1 \delta}} \leq \gamma$ is satisfied, it can proven that $y(t) \in \mathcal{D}$, $\forall t \in [t_0, \infty)$. The proper selection of control gains α, k_1, k_2, k_3, β, and Γ, and the selectable constant ε can guarantee that $y(t_0)$ lies within $\mathcal{S}_D$. The common Lyapunov-like function in (3.16) can be used with (3.26) to prove that $r, e_f, \tilde{\theta} \in \mathcal{L}_\infty$. Noting that x_d is user-defined and is bounded, and using (3.1) and (3.2) it can be shown that $e, x \in \mathcal{L}_\infty$. Using (2.4) and (3.10) and the fact that $\tilde{\theta} \in \mathcal{L}_\infty$, implies that $\hat{\theta} \in \mathcal{L}_\infty$. Additionally, utilizing Assumption 3.1 and (3.13), it can be proven that $\hat{g}_\phi, \hat{g}_\phi^+ \in \mathcal{L}_\infty$. Therefore, since $\dot{x}_d \in \mathcal{L}_\infty$ and from (3.13), it is clear that $u \in \mathcal{L}_\infty$. $\square$

3.3 Simulation

A series of simulations were performed to demonstrate the effectiveness of the proposed ARISE controller. To demonstrate ARISE's performance compared to SM control, simulations were performed using the developed ARISE controller and a traditional SM controller. The dynamics considered during the simulations were similar to a two-state Van der Pol oscillator; however, the dynamics were modified to be switched, to include disturbances, and to have a control-affine control input. Specifically, the unknown drift dynamics used in the simulations were

$$f_\sigma(x) = \begin{bmatrix} \mu\sigma\left(x_1 - \frac{1}{3}x_1^3 - x_2\right) \\ \frac{1}{\mu\sigma}x_1 \end{bmatrix},$$

where $\mu \in \mathbb{R}_{>0}$ is an unknown system parameter, $x = [x_1, x_2]^T$, and

$$\sigma = \begin{cases} 1, & x_1 \geq 0 \\ 2, & \text{otherwise} \end{cases} \tag{3.27}$$

is an unknown state-dependent switching signal that indicates the index of the drift dynamics. The disturbances used during the simulation were designed as

$$d(t) = \begin{bmatrix} d_1 \\ d_2 \end{bmatrix},$$

where $d_1, d_2 \in \mathbb{R}_{>0}$ are uncertain parameters. The control effective matrix used in the simulations was

$$g_\phi(x, t) = \begin{bmatrix} c_1\phi_1(x) + c_2\phi_2(x) & 0 \\ 0 & c_3\phi_1(x) + c_4\phi_2(x) \end{bmatrix},$$

where $c_1, c_2, c_3, c_4 \in \mathbb{R}$ are unknown, constant, and non-zero parameters, and

$$\phi_1(x) \triangleq \begin{cases} 1, & x_2 \geq 0 \\ 0, & \text{otherwise} \end{cases} \quad \text{and} \tag{3.28}$$

$$\phi_2(x) \triangleq (1 - \phi_1(x)) \tag{3.29}$$

are known state-dependent switching signals. The index of the control effectiveness matrix is

$$\phi = \begin{cases} 1, & \phi_1 = 1 \\ 2, & \phi_1 = 0 \end{cases},$$

based on the switching signals defined in (3.28) and (3.29). Additionally, using Assumption 2.4, the product $g_\phi u$ can be linearly parameterized as

$$g_\phi u = \underbrace{\begin{bmatrix} \phi_1 u_1 & (1-\phi_1)\, u_1 & 0 & 0 \\ 0 & 0 & \phi_1 u_2 & (1-\phi_1)\, u_2 \end{bmatrix}}_{Y} \underbrace{\begin{bmatrix} c_1 \\ c_2 \\ c_3 \\ c_4 \end{bmatrix}}_{\theta},$$

where $u = [u_1, u_2]^T$.

The initial conditions of the states and the desired trajectory for the simulation were $x(0) = \begin{bmatrix} 3 & 2 \end{bmatrix}^T$ and $x_d = [5\cos(t), 5\sin(t)]^T$, respectively. The control gains for the ARISE controller were selected as $\alpha = 0.1$, $k_1 = 3.5$, $k_2 = 100$, $k_3 = 20$, $\beta = 10$, and $\Gamma = \operatorname{diag}\{10, 20, 5, 15\}$. The parameter estimates were initialized as $\hat{\theta}(0) = \begin{bmatrix} 5 & 5 & 5 & 5 \end{bmatrix}^T$. The time step of 0.002 seconds was used in the simulation. Two sets of unknown constants were selected for the control effectiveness matrix to analyze the change in performance of the control law across varying parameter selections. For the first set, the values of c_1, c_2, c_3, and c_4 were selected as 5, 10, 3, and 6, respectively, and the set is named as $'\mathrm{GA}'$. For the other set of unknown constants, the parameters were respectively set as 7, 10, 3, and 4 and the set is named as $'\mathrm{GB}'$. Similarly, the performance of the control law was analyzed for 8 different sets of disturbances; 4 continuous disturbances and 4 constant disturbances, as presented in Table 3.1. The control performance was also analyzed for 7 different values of μ evenly spaced from 0.5 to 3.5. Analyzing the performance at different μ values helps to ensure the robustness of the controllers across varying dynamic parameters.

The SM controller that is used for comparative purposes in the simulations is defined as $u = \hat{g}_\phi^+(x(t), t)(-k_4 e(t) - k_5 \operatorname{sgn}(e) + \dot{x}_d(t))$, where k_4 is a robust control gain for the SM controller and k_5 is a SM control gain. The SM control gains were selected as $k_4 = 90$ and $k_5 = 3.5$. The listed gains for both controllers were adjusted using an empirical-based

Table 3.1: Continuous and constant disturbances used in simulation

Disturbances	d_1	d_2
a	0.5cos(t)	0.5sin(t)
b	0.1cos(t)	0.1sin(t)
c	0.05cos(t)	0.05sin(t)
d	0.01cos(t)	0.01sin(t)
e	0.5	0.5
f	0.1	0.1
g	0.05	0.05
h	0.01	0.01

method for a single set of dynamic parameters and disturbances (i.e $\mu = 1.5$, control effectiveness parameters = set $'\mathrm{GA}'$, and disturbances = set $'\mathrm{a}'$). First, the control gains for the ARISE controller were selected and then adjusted to achieve an improved performance (i.e., minimum tracking errors). After that, the control gains for the SM controller were selected and then adjusted similar to the ARISE controller gains. While selecting the control gains for the SM controller, similar gain values were considered to ensure a fair comparison between the two controllers. The selected control gain values were then used across all other dynamic sets during the simulations. Similar to the development of the ARISE adaptive update law, an adaptive update law was developed for the SM controller as $\dot{\hat{\theta}}(t) \triangleq \mathrm{Proj}\left(\Gamma Y_\phi^T\left(x\left(t\right), t, u\left(t\right)\right) e\left(t\right)\right)$ was implemented to the SM control architecture. The initial estimates of θ and the gain Γ were selected to be the same for the ARISE and SM controllers. The RMS of the tracking errors were evaluated for both controllers to compare their effectiveness, thereby providing valuable insights into their robustness when implemented on a switched system.

3.4 Results/Discussion

The aforementioned simulations demonstrate the capability of the proposed ARISE control system for a switched dynamic system. Figure 3.1 depicts the tracking errors of the ARISE and SM controllers for a single set of dynamic parameters and disturbance inputs, highlighting the different tracking performance between the two controllers. The results in Figure 3.1

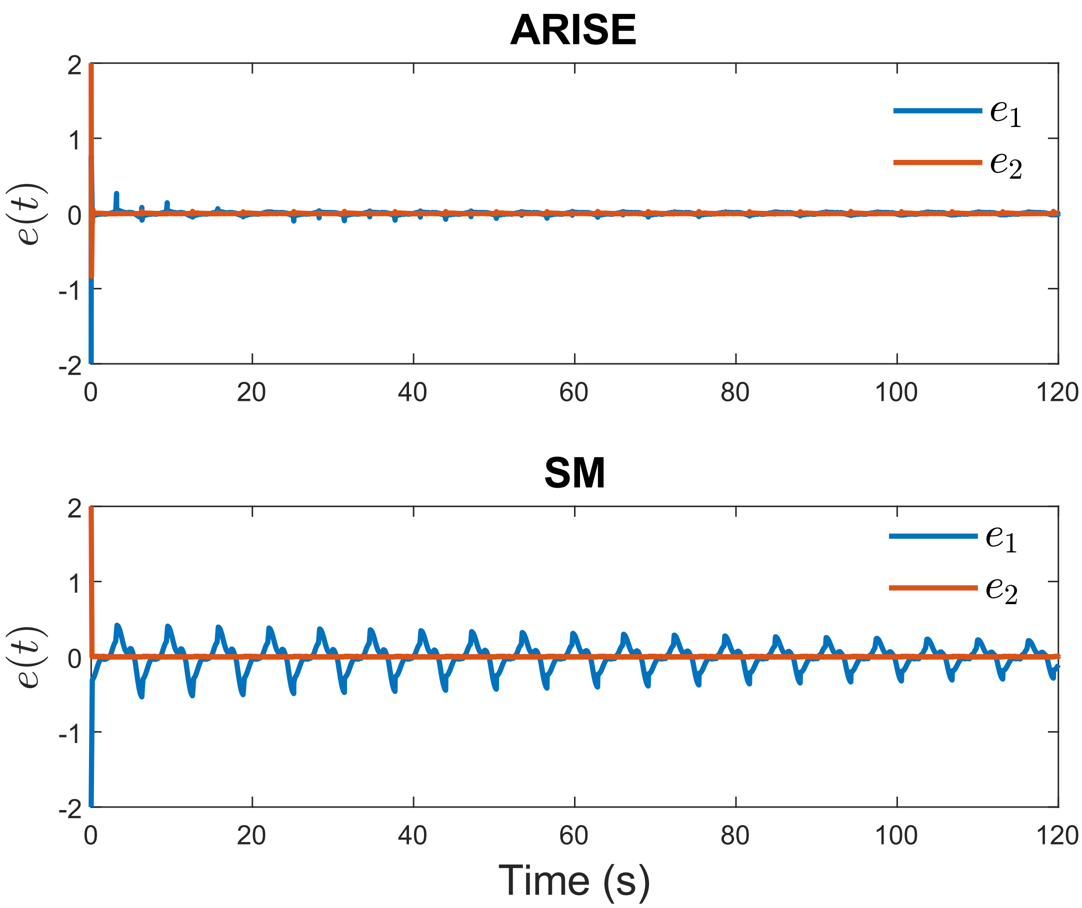

Figure 3.1: Tracking error comparison for the parameters $\mu = 1.5$, $c_1 = 7$, $c_2 = 10$, $c_3 = 3$, $c_4 = 4$ (i.e., set $'$GB$'$), $d_1 = 0.5\cos(t)$, and $d_2 = 0.5\sin(t)$ (i.e., set $'$a$'$).

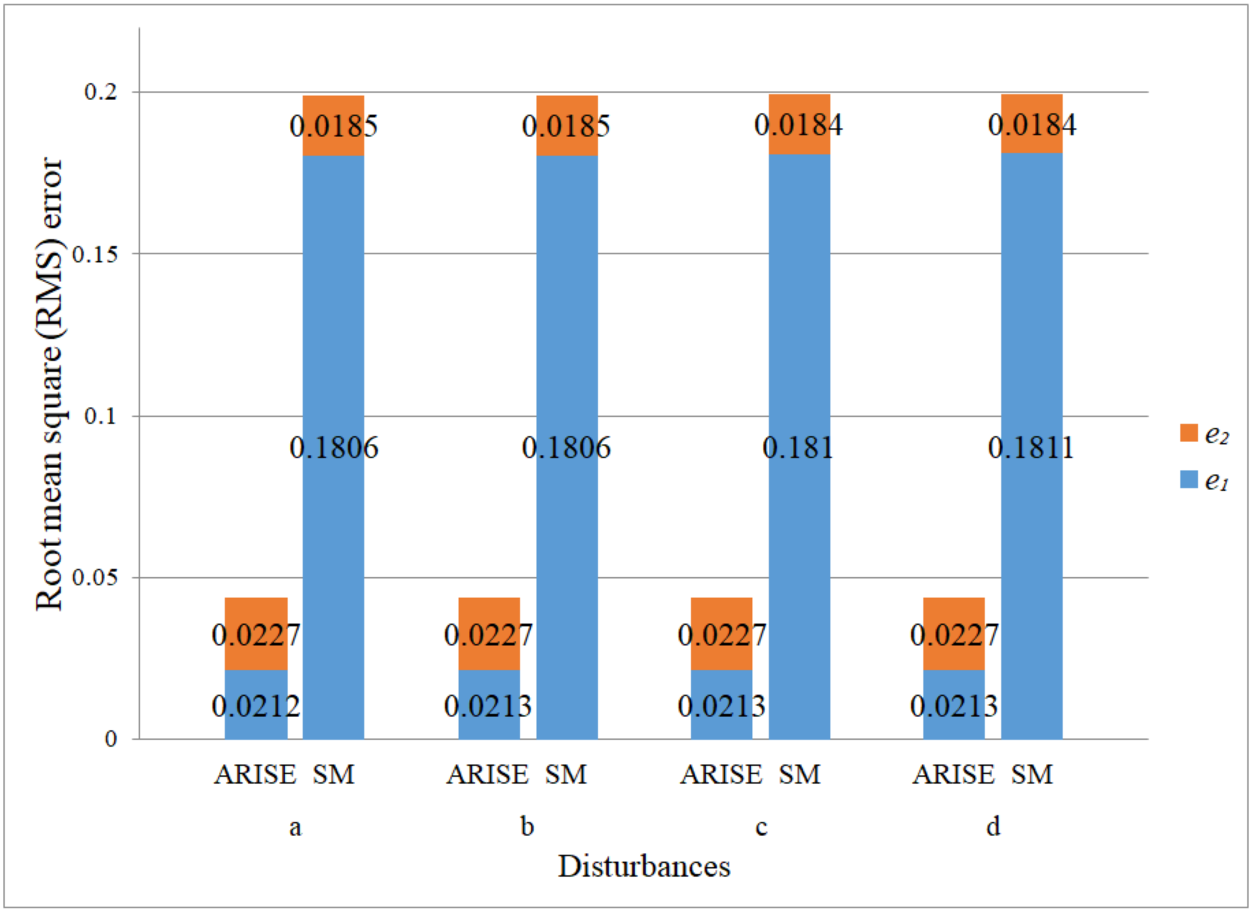

Figure 3.2: RMS tracking errors across varying continuous disturbances when $\mu = 1.5$, $c_1 = 5$, $c_2 = 10$, $c_3 = 3$, and $c_4 = 6$ (i.e., set $'$GA$'$). The terms $'$a$'$-$'$d$'$ refer to the disturbance configurations in Table 3.1.

are representative across all dynamic parameter sets and disturbances that were considered. By referencing Figure 3.1, it is observed that the tracking errors decreased with increasing time for both ARISE and SM, which is likely due to the improving estimate of θ due to the adaptive update laws. However, the convergence in the proposed ARISE controller was better than the SM controller, which is likely due to the the ARISE controller implementing an integral SM term rather than a discontinuous SM term. The RMS tracking errors for both of the controllers were analyzed across varying sets of continuous disturbances (see Table 3.1) and the results for a single set of dynamic parameters are presented in Figure 3.2. Referencing Figure 3.2, it is clear that the RMS errors across different disturbance values for both controllers were consistent. However, the ARISE controller exhibited considerably

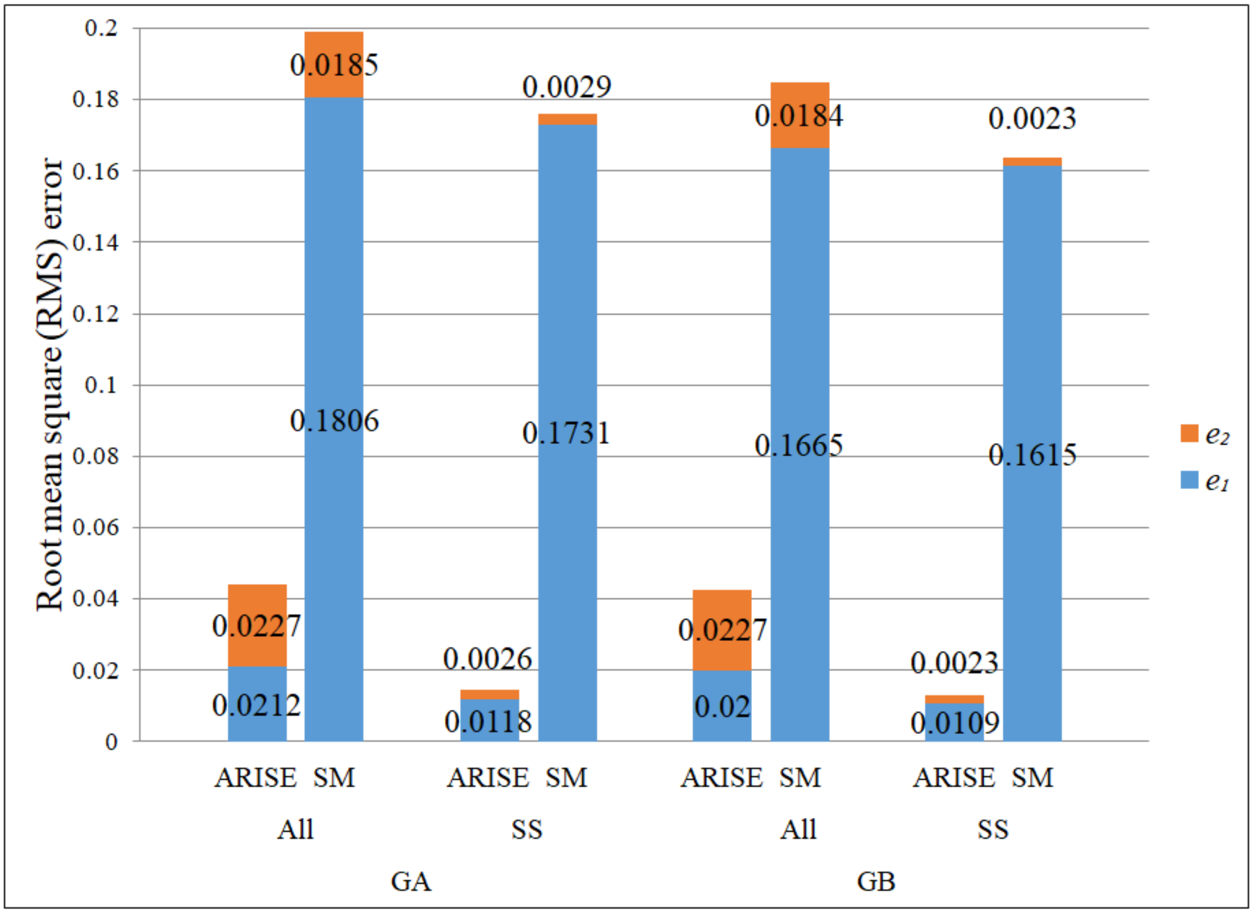

Figure 3.3: RMS tracking errors across varying dynamic when $\mu = 1.5$, $d_1 = 0.5\cos(t)$, and $d_2 = 0.5\sin(t)$. The RMS error of a system after steady state (SS) was also evaluated. The state of the system after 10 seconds is considered as SS. The $'$GA$'$ dynamic parameters are $c_1 = 5$, $c_2 = 10$, $c_3 = 3$, and $c_4 = 6$ and the $'$GB$'$ dynamic parameters are $c_1 = 7$, $c_2 = 10$, $c_3 = 3$, and $c_4 = 4$.

smaller RMS errors than the SM controller, which indicates that the ARISE controller has a better tracking performance than SM control. When the process to generate Figure 3.2 was repeated using the constant disturbances in Table 3.1 ($'$e$'$-$'$h$'$), similar results were obtained for both controllers (i.e., the results for $'$a$'$ and $'$e$'$, $'$b$'$ and $'$f$'$, and so on were nearly identical) and thus the figure is omitted. Likewise, Figure 3.3 presents the RMS tracking errors for both controllers under different control effectiveness values (i.e., $'$GA$'$ and $'$GB$'$), and a single set of dynamic parameters and disturbances. The RMS errors of the system once it reaches steady state (SS) are also illustrated in Figure 3.3. Figure 3.3 depicts that the RMS errors of the ARISE controller were smaller than the SM controller even across

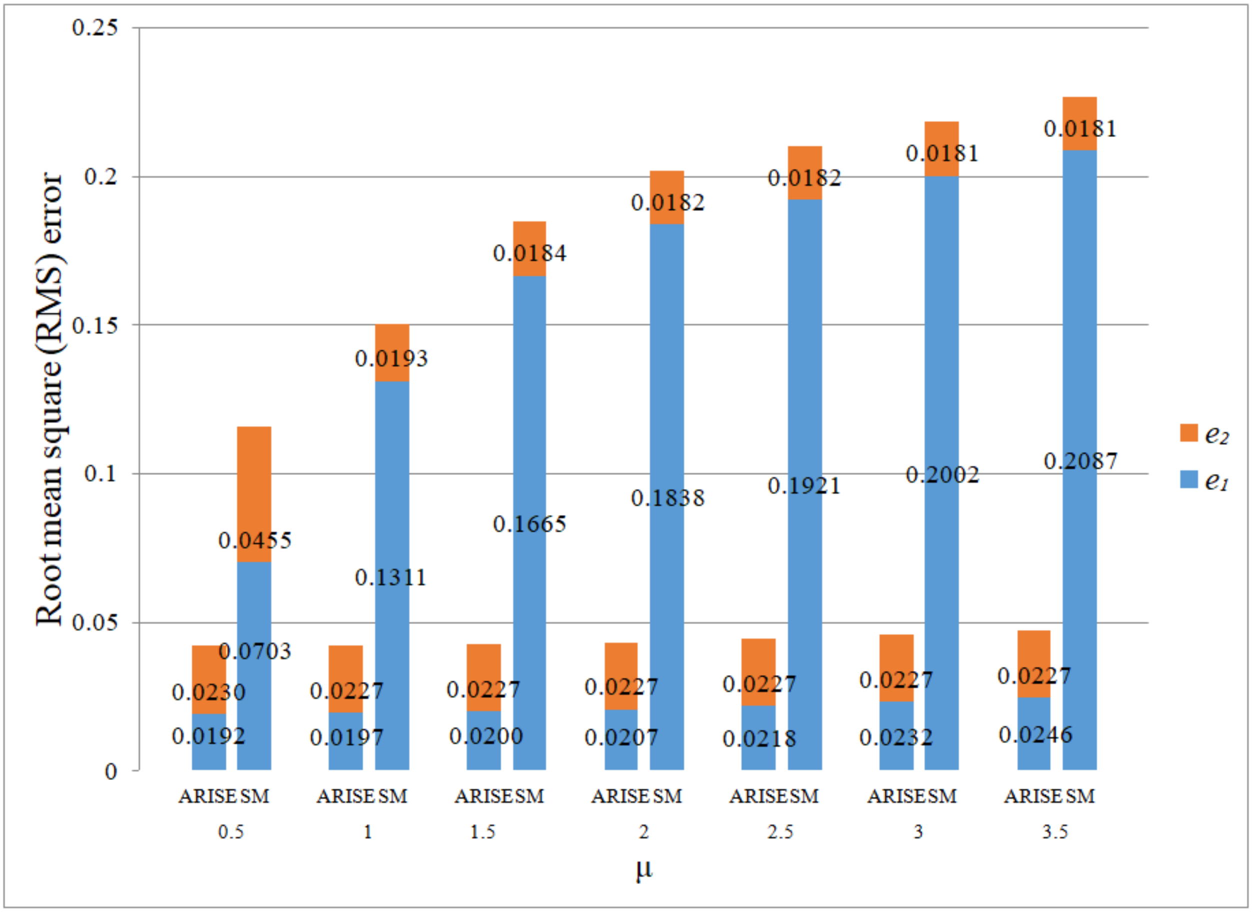

Figure 3.4: RMS tracking errors across varying values for the dynamic parameter μ when $c_1 = 7$, $c_2 = 10$, $c_3 = 3$, $c_4 = 4$ (i.e., set $'\mathrm{GB}'$), $d_1 = 0.5\cos(t)$, and $d_2 = 0.5\sin(t)$ (i.e., set $'\mathrm{a}'$).

varying control effectiveness parameters, thereby indicating that the ARISE controller performs better on a switched system. Furthermore, there was a notable decrease in the RMS errors of the second state for both controllers once the system reached SS as illustrated in Figure 3.3. This result may be due to the second state having fewer nonlinearities associated with its dynamic model. Moreover, Figure 3.4 depicts the RMS tracking errors for both controllers when varying the parameter μ. Referencing this figure, the RMS errors of the ARISE controller increased negligibly with increasing values of μ. Comparatively, the RMS errors of the SM controller significantly increased with increasing values of μ. This consistent performance of the ARISE controller despite changing the dynamic parameter suggests that ARISE is more robust than SM control when implemented on a switched system. It is also noticeable from Figure 3.4 that the magnitude of the RMS errors associated with ARISE were always smaller than the errors from the SM controller, further demonstrating the ARISE controller's effectiveness over SM control.

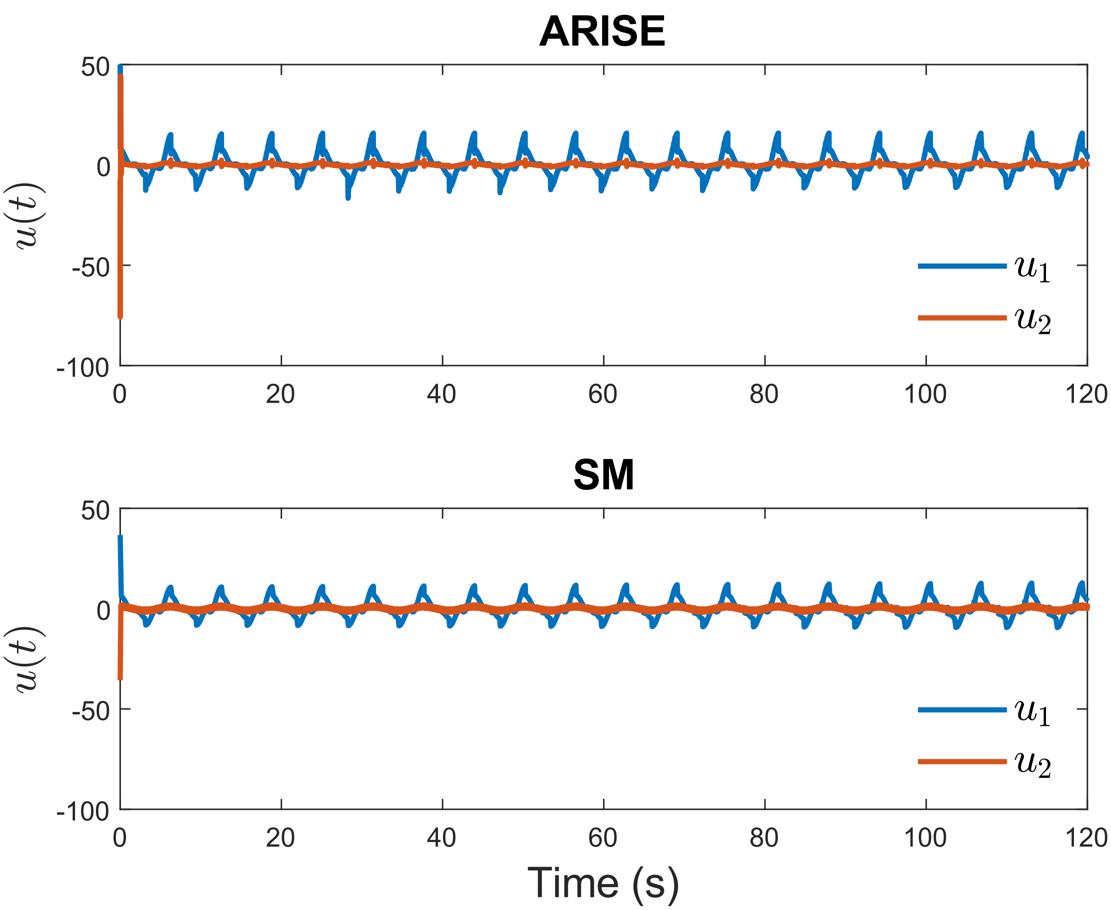

Figure 3.5: Control input comparisons when $\mu = 1.5$, $c_1 = 7$, $c_2 = 10$, $c_3 = 3$, $c_4 = 4$ (i.e., set $'\mathrm{GB}'$), $d_1 = 0.5\cos(t)$, and $d_2 = 0.5\sin(t)$ (i.e., set $'\mathrm{a}'$).

A representative depiction of the control inputs for both controllers is presented in Figure 3.5 for a single set of dynamics and disturbances. The proposed ARISE controller having reduced the tracking errors required a similar (although slightly larger) amount of control input compared to the SM controller. Figure 3.6 is generated by narrowing Figure 3.5 to view the control inputs across a narrow subset of time. Referencing Figure 3.6, the SM controller exhibits a rapid switching within the control input, which induces the chattering effect. Conversely, the ARISE controller displays a smoother control input, effectively mitigating

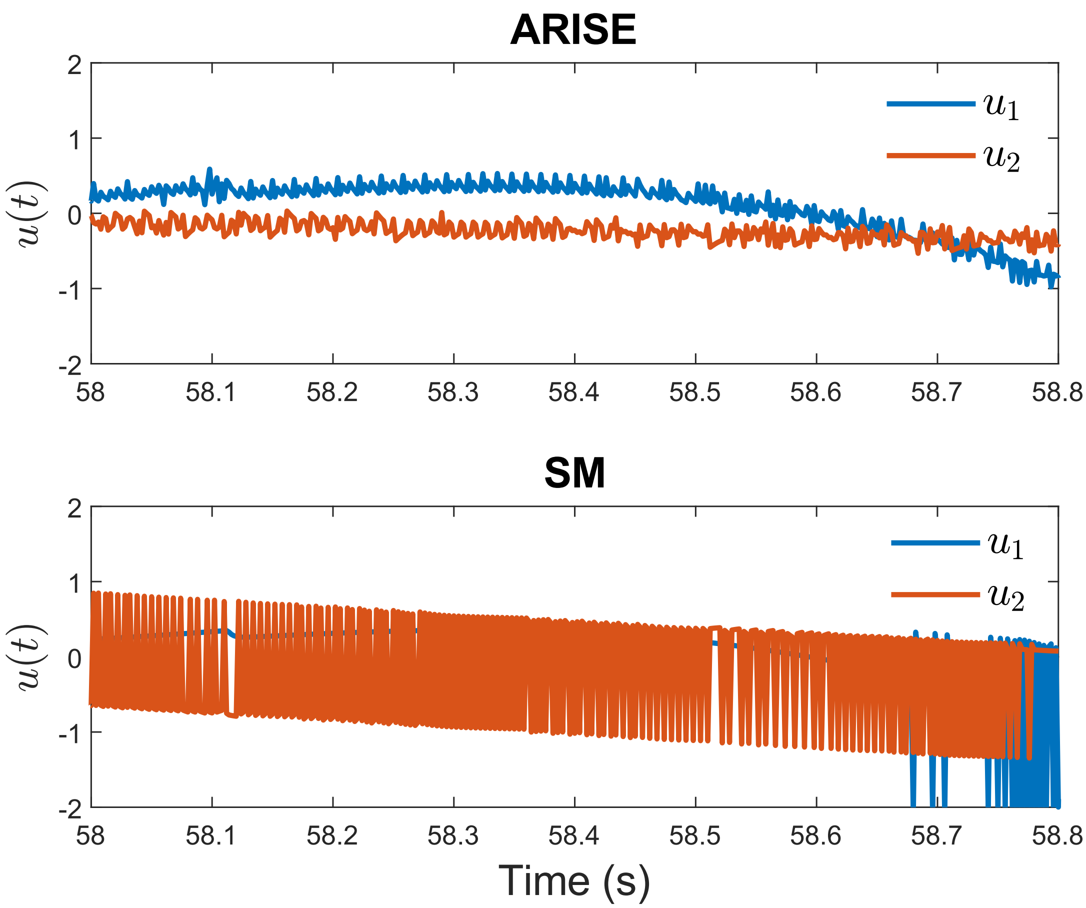

Figure 3.6: Control input comparisons showing the cause of chattering in SM control when $\mu = 1.5$, $c_1 = 7$, $c_2 = 10$, $c_3 = 3$, $c_4 = 4$ (i.e., set $'\mathrm{GB}'$), $d_1 = 0.5\cos(t)$, and $d_2 = 0.5\sin(t)$ (i.e., set $'\mathrm{a}'$).

the chattering effect. A key contribution of the proposed controller is that it is able to control a nonsmooth system unlike traditional RISE controllers. Even though RISE controllers also use an integral SM term similar to ARISE, it can only be implemented on differentiable or smooth dynamic systems. The ARISE controller, on the other hand, obtains the benefits of RISE while being implementable on a wider class of dynamic systems.

It should furthermore be noted that SM control is capable of achieving exponential tracking of the considered dynamic system; whereas, ARISE control is only able to achieve uniformly ultimately bounded tracking of the same system. Despite the theoretical limitations of the ARISE approach, its tracking performance was superior to SM control in simulation. It is anticipated that the improved performance of the ARISE controller compared to SM control will be more substantial in experimentation since real actuators are unable to perfectly implement SM control signals due to their requirement for infinite control frequency.

3.5 Concluding Remarks

This chapter answered the motivating question through the development of a novel filtered error system that injects a SM term indirectly into the open-loop error system. The ARISE controller, which is implementable in switched and nonsmooth dynamic systems, was developed by introducing a novel filtered error system. The control law developed in this chapter ensured semi-global exponential tracking to an ultimate bound, provided that feasible gain and initial conditions were satisfied. The simulation results ensure that the proposed ARISE controller is capable of controlling a switched system while reducing chatter. The comparison results between the ARISE and the standard SM controllers show that the ARISE controller's tracking performance was superior to SM control while simulating in a switched system, indicating that the ARISE controller can be efficient for switched systems.

Chapter 4

Saturated ARISE Controller

In this chapter, the development process for a saturated ARISE controller is presented. Specifically, this chapter seeks to extend the result in Chapter 3 by modifying the control development and stability analysis to develop a saturated version of the ARISE controller. A limitation of the previously developed ARISE controller from Chapter 3 is that its control architecture demands excessive control effort whenever the state errors are great in magnitude akin to standard high-gain robust controllers. This excessive control input can hinder the practicality of ARISE controllers because the control requirement may exceed the physical limitations of certain actuators. Specifically, large uncertain disturbances and initial conditions that deviate greatly from the desired trajectory will demand a high control input signal that may require control inputs that go beyond the physical capabilities of the system's actuators, essentially establishing an impromptu saturation limit during the transient response [60]. This unplanned actuator saturation will not only degrade the overall performance of the controller, but it also poses a potential mechanical risk and may result in thermal failure in physical systems, preventing the adoption of ARISE controllers in safety-critical applications [61, 62, 63].

In this chapter, a saturated ARISE control scheme that accounts for the limitations of an actuator, while being robust to the system uncertainties and disturbances, is developed for a control-affine nonlinear system as in the authors preliminary work in [64]. This saturated ARISE controller incorporates smooth hyperbolic tangent functions as the saturation function within the control input and invokes adaptive techniques to learn the system's uncertainties, and to ensure system stability and convergence. Specifically, control effectiveness matrix used in the dynamics is considered to be unknown and potentially nonsmooth and switched, and it is estimated using an adaptive control approach. To enhance real-world applicability and to eliminate the risk of actuation failure, the feedback control gains associated with the hyperbolic terms can be adjusted to bound the control inputs a priori based on the physical constraints or specifications of each actuator. Furthermore, a novel filtered error system was developed in this work to inject a signum function into the closed-loop error system. A nonsmooth Lyapunov-like stability analysis is performed to prove uniformly ultimately bounded tracking of a desired trajectory. A particular benefit of the developed saturated controller is that the control input can be bounded a priori, which enables the control gains to be designed around limitations of the actuator.

A series of numerical simulations were performed to analyze the effectiveness of the saturated ARISE controller and its performance was compared with a saturated SM controller. The numerical simulations were performed using a modified two-state Van der Pol oscillator as the dynamic model. The oscillator was modified to be switched and to include control-affine control inputs. To evaluate the effectiveness of the controllers, the root mean square (RMS) errors were determined for both of the controllers across varying dynamic parameters. While evaluating the RMS errors, it was concluded that the RMS errors of the saturated ARISE controller were smaller than the RMS errors of the saturated SM controller, which proves that the proposed saturated ARISE controller is more robust than the SM controller. Hence, the better performance of the saturated ARISE controller validated its superiority over the standard saturated SM controller for the considered switched system.

4.1 Control Development

The control objective in this work is to design a saturated controller that ensures the generalized states, $x(t)$ in the dynamics in (2.1), track a sufficiently smooth desired time-varying trajectory $x_d(t) : \mathbb{R}_{\geq 0} \to \mathbb{R}^n$, despite having uncertainties and unknown disturbances within the system dynamics. The desired trajectory and its derivative are considered to be known and bounded such that $x_d(t), \dot{x}_d(t) \in \mathcal{L}_\infty$. To quantify the control objective, a tracking error denoted as $e : \mathbb{R}_{\geq 0} \to \mathbb{R}^n$ is defined as

$$e(t) \triangleq x(t) - x_d(t). \tag{4.1}$$

Another objective of this work is to inject a SM term into the open-loop error system without introducing it in the controller. This objective is accomplished by designing a measurable auxiliary error, denoted by $r : \mathbb{R}_{\geq 0} \to \mathbb{R}^n$, that is defined as

$$r(t) \triangleq e(t) + \alpha \mathrm{Tanh}(e_f(t)), \tag{4.2}$$

where $\alpha \in \mathbb{R}_{>0}$ denotes a user-defined control gain and $e_f : \mathbb{R}_{\geq 0} \to \mathbb{R}^n$ denotes an auxiliary filtered error signal that is defined as $e_f(t) \triangleq [e_{f,1}(t), \ldots, e_{f,n}(t)]^T$. The term $\mathrm{Tanh}(e_f(t)) : \mathbb{R}^n \to \mathbb{R}^n$ in (4.2) is a vector of hyperbolic tangent functions that facilitate the saturated control design and is defined as

$$\mathrm{Tanh}(e_f(t)) \triangleq \begin{bmatrix} \tanh(e_{f,1}(t)) \\ \tanh(e_{f,2}(t)) \\ \vdots \\ \tanh(e_{f,n}(t)) \end{bmatrix}. \tag{4.3}$$

The time derivative of the auxiliary filtered error is defined as

$$\dot{e}_f(t) \triangleq \mathrm{Cosh}^2(e_f(t)) \left(-k_1 \mathrm{sgn}(r(t)) - k_2 r(t) - \beta \mathrm{Tanh}(e_f(t))\right), \tag{4.4}$$

where $k_1, k_2, \beta \in \mathbb{R}_{>0}$ are user-defined control gains, $\mathrm{sgn}(\cdot)$ denotes the signum function, and $\mathrm{Cosh}(e_f(t)) : \mathbb{R}^n \to \mathbb{R}^{n \times n}$ is a diagonal matrix of hyperbolic cosine functions that is defined as

$$\operatorname{Cosh}(e_f) \triangleq \operatorname{diag}\{\cosh(e_{f,1}), \ldots, \cosh(e_{f,n})\}. \tag{4.5}$$

Note that the derivative of the auxiliary error signal, $\dot{e}_f(t)$, has the SM term, which implies that the auxiliary error, $e_f(t)$, has an integral of the SM term. The integral SM term will be included in the control law through $e_f(t)$. Additionally, the initial condition for the auxiliary error signal can be chosen as $e_f(t_0) = 0_{n\times 1}$, where $0_{n\times 1}$ is a vector of n numbers of zero. Subsequently, taking the time derivative of (4.2) and using (2.1), (4.1), and (4.4) yields

$$\dot{r}(t) = f_\sigma(x(t)) + d_\sigma(t) + \tau_\phi(x(t), t) - \dot{x}_d(t) - \alpha k_1 \operatorname{sgn}(r(t)) - \alpha k_2 r(t) - \alpha\beta \operatorname{Tanh}(e_f(t)). \tag{4.6}$$

Using (2.2) with (4.6) yields an error function as

$$\dot{r}(t) = \chi_\sigma(t) + g_\phi(x(t), t)\, u(t) - \dot{x}_d(t) - \alpha k_1 \operatorname{sgn}(r(t)) - \alpha k_2 r(t) - \alpha\beta \operatorname{Tanh}(e_f(t)), \tag{4.7}$$

where $\chi_\sigma : \mathbb{R}_{\geq 0} \to \mathbb{R}^n$ is an auxiliary term defined as

$$\chi_\sigma(t) \triangleq f_\sigma(x(t)) + d_\sigma(t). \tag{4.8}$$

The auxiliary term can be upper bounded using Assumptions 2.1 and 2.2 and Equations (4.1) and (4.2) as

$$\|\chi_\sigma(t)\| \leq \Phi + \rho(\|z(t)\|)\, \|z(t)\|, \tag{4.9}$$

where $\rho(\cdot)$ is a strictly increasing radially unbounded known positive function, $\Phi \in \mathbb{R}_{>0}$ is a known constant, and $z : \mathbb{R}_{\geq 0} \to \mathbb{R}^{2n}$ is a composite error vector defined as

$$z(t) \triangleq \begin{bmatrix} r^T(t) & \operatorname{Tanh}^T(e_f(t)) \end{bmatrix}^T. \tag{4.10}$$

To facilitate the development of the controller, an estimation of the unknown control effectiveness matrix is done by estimating the generalized torque $\hat{\tau}_\phi(x(t), t) = \hat{g}_\phi(x(t), t) u(t)$, where $\hat{g}_\phi : \mathbb{R}^n \times \mathbb{R}_{\geq 0} \to \mathbb{R}^{n \times m}$ is an estimate of the control effectiveness matrix. As per Assumption 2.4, the estimate of the generalized torque can be linearly parameterized as

$$\hat{g}_\phi(x(t), t) u(t) = Y_\phi(x(t), t, u(t)) \hat{\theta}(t), \tag{4.11}$$

where $\hat{\theta} : \mathbb{R}_{\geq 0} \to \mathbb{R}^q$ is an estimate of the unknown vector of constants θ. The mismatch between the uncertain parameters and their estimates results in a parameter estimate error denoted as $\tilde{\theta} : \mathbb{R}_{\geq 0} \to \mathbb{R}^q$, that is defined as

$$\tilde{\theta}(t) \triangleq \theta - \hat{\theta}(t). \tag{4.12}$$

Assumption 4.1. *The estimate of the control effectiveness matrix* $\hat{g}_\phi(x(t), t), \forall t \geq t_0$ *is a full-row rank matrix that is bounded such that* $\hat{g}_\phi(x(t), t) \in \mathcal{L}_\infty$ *provided that the parameter estimates* $\hat{\theta}(t)$ *and system states* $x(t)$ *are bounded such that* $\hat{\theta}(t), x(t) \in \mathcal{L}_\infty$. *Consequently, the right pseudo inverse, denoted as* $\hat{g}_\phi^+ : \mathbb{R}^n \times \mathbb{R}_{\geq 0} \to \mathbb{R}^{m \times n}$ *and defined as* $\hat{g}_\phi^+(\cdot) \triangleq \hat{g}_\phi^T(\cdot)\left(\hat{g}_\phi(\cdot)\hat{g}_\phi^T(\cdot)\right)^{-1}$, *exists and can be bounded a priori provided that* $\hat{\theta}(t)$ *satisfies the bounds for theta defined in* (2.4).

Adding and subtracting $Y_\phi(x(t), t, u(t)) \hat{\theta}(t)$ in (4.7) and using (2.3), (4.11), and (4.12) yields the open-loop error dynamics as

$$\begin{aligned} \dot{r}(t) &= \chi_\sigma(t) + Y_\phi(x(t), t, u(t)) \tilde{\theta}(t) + \hat{g}_\phi(x(t), t) u(t) \\ &\quad - \dot{x}_d(t) - \alpha k_1 \operatorname{sgn}(r(t)) - \alpha k_2 r(t) - \alpha\beta \operatorname{Tanh}(e_f(t)). \end{aligned} \tag{4.13}$$

Referencing the open-loop error law in (4.13), the control input is defined as

$$u(t) \triangleq \hat{g}_\phi^+(x(t), t)\left[(k_2 + \alpha\beta) \operatorname{Tanh}(e_f(t)) + \dot{x}_d(t)\right]. \tag{4.14}$$

Similarly, the parameter estimate law is designed as

$$\dot{\hat{\theta}}(t) \triangleq \mathrm{Proj}\left(\Gamma Y_{\phi}^{T}(x(t), t, u(t))\, r(t)\right), \tag{4.15}$$

where $\mathrm{Proj}(\cdot)$ denotes a smooth projection algorithm defined in [57] and $\Gamma \in \mathbb{R}^{q\times q}$ denotes a positive definite diagonal gain matrix. The projection algorithm ensures that the estimate of unknown parameters $\hat{\theta}(t)$ stays within the known bounds defined in (2.4) for $\theta(t)$. The proposed controller in (4.14) can be bounded a priori based on (4.15) and Assumption 4.1. Substituting the controller from (4.14) into the open-loop error system in (4.13) yields the closed-loop error system as

$$\dot{r}(t) = Y_{\phi}(x(t), t, u(t))\, \tilde{\theta}(t) - \alpha k_2 r(t) - \alpha k_1 \mathrm{sgn}(r(t)) + k_2 \mathrm{Tanh}(e_f(t)) + \chi_{\sigma}(t). \tag{4.16}$$

Referencing the closed-loop error system in (4.16), the equation contains a SM term due to the introduction of the auxiliary filter error $e_f(t)$, which helps to deal with the uncertainties within the dynamics that are upper bounded by a constant. In turn, the signal $\mathrm{Tanh}(e_f(t))$ injects a saturated integral of the signum function within the control input, which produces a continuous integral SM-like term in the controller and reduces chattering. Moreover, including $\mathrm{Tanh}(e_f(t))$ within the control architecture has the added benefit of accounting for actuator limitations.

4.2 Stability Analysis

For the subsequent stability analysis, let the i^{th} time when ϕ switches to $w \in \mathcal{S}$ be represented as $\{t_i^{w,\text{on}}\}, \forall i \in \mathbb{N}$, and the i^{th} time when ϕ switches from $w \in \mathcal{S}$ be represented as $\left\{t_i^{w,\text{off}}\right\}$, $\forall i \in \mathbb{N}$. Consider a continuously differentiable and positive definite common Lyapunov function candidate, $V_L : \mathcal{D} \times \mathbb{R}_{\geq 0} \to \mathbb{R}_{\geq 0}$ that is defined as[1]

$$V_L(y,t) \triangleq \frac{1}{2} r^T r + \frac{1}{2} \mathrm{Tanh}^T(e_f)\, \mathrm{Tanh}(e_f) + \frac{1}{2} \tilde{\theta}^T \Gamma^{-1} \tilde{\theta}, \tag{4.17}$$

where the domain $\mathcal{D} \subseteq \mathbb{R}^{2n+q}$ is defined as $\mathcal{D} \triangleq \left\{ y \in \mathbb{R}^{2n+q} \,|\, \|y\| \leq \gamma \right\}$, $\gamma \in \mathbb{R}_{>0}$ is a known constant that satisfies the inequality[2] $\gamma \leq \inf\left\{ \rho^{-1}\left(\left(\sqrt{\alpha k_2 \delta}, \infty \right) \right) \right\}$, $\delta \in \mathbb{R}$ is a known constant defined as $\delta \triangleq \min\left(\frac{1}{2}\alpha k_2,\ \beta - \frac{\varepsilon k_1}{2} \right)$, $\varepsilon \in \mathbb{R}_{>0}$ is a selectable constant, and $y : \mathbb{R}_{\geq 0} \to \mathbb{R}^{2n+q}$ is the concatenated state vector defined as

$$y \triangleq \begin{bmatrix} z^T & \tilde{\theta}^T \end{bmatrix}^T. \tag{4.18}$$

The Lyapunov function candidate V_L can be lower and upper bounded using the norm of the concatenated state vector y as

$$\lambda_1 \|y\|^2 \leq V_L \leq \lambda_2 \|y\|^2, \tag{4.19}$$

where the constants λ_1,$\lambda_2 \in \mathbb{R}_{\geq 0}$ are defined as $\lambda_1 \triangleq \min\left(\frac{1}{2}, \frac{1}{2}\lambda_{\min}\left\{ \Gamma^{-1} \right\} \right)$ and $\lambda_2 \triangleq \max\left(\frac{1}{2}, \frac{1}{2}\lambda_{\max}\left\{ \Gamma^{-1} \right\} \right)$. The terms $\lambda_{\min}\{\cdot\}$ and $\lambda_{\max}\{\cdot\}$ are defined as the minimum and maximum eigenvalues of $\{\cdot\}$, respectively. The Lyapunov function candidate V_L can further be bounded using the composite error vector z as

$$\frac{1}{2} \|z\|^2 \leq V_L \leq \frac{1}{2} \|z\|^2 + v_1. \tag{4.20}$$

In the inequality in (4.20), the term $v_1 : \mathbb{R}^q \to \mathbb{R}_{\geq 0}$ is defined as

$$v_1 \triangleq \frac{1}{2} \lambda_{\max}\left\{ \Gamma^{-1} \right\} \left\| \tilde{\theta} \right\|_{\max}^2, \tag{4.21}$$

[1]For notational brevity, all functional dependencies are hereafter suppressed unless required for clarity of exposition.

[2]For a set B, the inverse image is defined as $\rho^{-1}(B) \triangleq \{ a \mid \rho(a) \in B \}$.

where $\left\|\tilde{\theta}\right\|_{\max} \in \mathbb{R}_{>0}$ is the maximum value of $\left\|\tilde{\theta}(t)\right\|$ such that $\left\|\tilde{\theta}(t)\right\| \leq \left\|\tilde{\theta}\right\|_{max}, \forall t \geq t_0$. It is important to note that the upper bound of $\tilde{\theta}(t)$ exists because of the $\operatorname{Proj}(\cdot)$ algorithm in (4.15) and the bounds defined in (2.4). Moreover, the set of allowable initial conditions, denoted by $\mathcal{S}_{\mathcal{D}} \subseteq \mathbb{R}^{2n+q}$, that facilitate the stability analysis is defined as

$$\mathcal{S}_{\mathcal{D}} \triangleq \left\{ y(t_0) \in \mathbb{R}^{2n+q} \,\middle|\, \sqrt{\lambda_2 \lambda_1^{-1}} \left\| y(t_0) \right\| \leq \gamma \right\}. \tag{4.22}$$

Theorem 4.1. *For the unknown, nonsmooth, and nonlinear dynamics in* (2.1) *that satisfy all Assumptions, the control input in* (4.14) *and parameter update law in* (4.15) *yield a uniformly ultimately bounded tracking result in the sense that*

$$\left\| y(t) \right\|^2 \leq \tfrac{\lambda_2}{\lambda_1} \left\| y(t_0) \right\|^2 \exp\left(-\delta (t - t_0)\right) + \tfrac{v}{\lambda_1 \delta} \left(1 - \exp\left(-\delta (t - t_0)\right)\right), \tag{4.23}$$

for all $t \in [t_0, \infty)$*, provided that* $y(t_0) \in S_{\mathcal{D}}$*, where* $v \triangleq \delta v_1 + \frac{n k_1}{2\varepsilon}$*, and provided that the following gain conditions are satisfied:*

$$\beta > \frac{\varepsilon k_1}{2}, \quad \alpha k_1 \geq \Phi, \quad \sqrt{\frac{v}{\lambda_1 \delta}} \leq \gamma. \tag{4.24}$$

Proof. The time-derivative of (4.17) exists almost everywhere (a.e.) within $t \in [t_0, \infty)$ because of the discontinuities in the closed-loop error system in (4.16). Let $y(t)$ be the Filippov solution of the differential inclusion $\dot{y} \in K[h](y)$ for all $t \in [t_0, \infty)$, where $h : \mathbb{R}^{2n+q} \to \mathbb{R}^{2n+q}$ is defined as $h(y) \triangleq \begin{bmatrix} \dot{r}^T, & \left(\frac{d}{dt}\operatorname{Tanh}(e_f)\right)^T, & \dot{\tilde{\theta}}^T \end{bmatrix}^T$ and $K[\cdot]$ is defined in [58].

Consider times when $\phi = w$ for some arbitrary $w \in S$ (i.e., $t \in \left[t_i^{w,\mathrm{on}}, t_i^{w,\mathrm{off}}\right)$ for some $i \in \mathbb{N}$), such that the dynamic functions Y_ϕ, g_ϕ, and $\hat{g}_\phi$ are continuous and $K[Y_\phi] = Y_\phi$, $K[g_\phi] = g_\phi$, and $K[\hat{g}_\phi] = \hat{g}_\phi$. Taking the generalized time derivative of the Lyapunov function candidate in (4.17), using the calculus of $K[.]$ from [59], and using equations (4.4), (4.12), (4.15), and (4.16) yields

$$\begin{aligned}\dot{\tilde{V}}_L \quad \subseteq \quad & r^T\left(K\left[\chi_\sigma\right]+Y_\phi\tilde{\theta}-\alpha k_2 r-\alpha k_1 K\left[\operatorname{sgn}\left(r\right)\right]+k_2\operatorname{Tanh}\left(e_f\right)\right) \\ & +\operatorname{Tanh}^T\left(e_f\right)\left(-k_1 K\left[\operatorname{sgn}\left(r\right)\right]-k_2 r-\beta\operatorname{Tanh}\left(e_f\right)\right)-\tilde{\theta}^T\Gamma^{-1}\left(\Gamma Y_\phi^T r\right).\end{aligned} \tag{4.25}$$

Upper bounding terms in (4.25), using (4.9) and (4.24), applying Young's Inequality, completing the squares, canceling common terms, and using facts like $\dot{V}_L\left(y\right) \overset{\text{a.e.}}{\in} \dot{\tilde{V}}_L\left(y\right)$, $\left\|K\left[\operatorname{sgn}\left(r\right)\right]\right\| \leq \sqrt{n}$, and $\|z\| \leq \|y\|$ yields

$$\dot{V}_L \overset{\text{a.e.}}{\leq} -\tfrac{1}{2}\alpha k_2\left\|r\right\|^2-\left(\beta-\tfrac{\varepsilon k_1}{2}\right)\left\|\operatorname{Tanh}\left(e_f\right)\right\|^2+\tfrac{1}{2\alpha k_2}\rho^2\left(\|y\|\right)\|z\|^2+\tfrac{nk_1}{2\varepsilon}. \tag{4.26}$$

Additionally, (4.26) can be further upper bounded using (4.10), (4.20), $v \triangleq \delta v_1+\frac{nk_1}{2\varepsilon}$, and $\delta \triangleq \min\left(k_3,\ \beta-\frac{\varepsilon k_1}{2}\right)$ to yield

$$\dot{V}_L \overset{\text{a.e.}}{\leq} -\delta V_L+v, \forall t \in \left[t_i^{w,\text{on}}, t_i^{w,\text{off}}\right) \tag{4.27}$$

assuming that $y\left(t\right) \in \mathcal{D}$, $\forall t \in \left[t_i^{w,\text{on}}, t_i^{w,\text{off}}\right)$. Since $\dot{V}_L$ is bounded for any arbitrary $\phi \in \mathcal{S}$, it can be bounded for all $\phi \in \mathcal{S}$, indicating that (4.27) holds true for all $t \in [t_0,\infty)$, assuming that $y\left(t\right) \in \mathcal{D}$, $\forall t \in [t_0,\infty)$. Hence, (4.17) can be considered as a common Lyapunov-like function for $t \in [t_0,\infty)$. The inequality in (4.27) can be further solved to yield

$$V_L\left(t\right) \leq \left(V_L\left(t_0\right)-\frac{v}{\delta}\right)\exp\left(-\delta\left(t-t_0\right)\right)+\frac{v}{\delta}, \tag{4.28}$$

$\forall t \in [t_0,\infty)$, assuming that $y\left(t\right) \in \mathcal{D}$, $\forall t \in [t_0,\infty)$. Provided that the gain condition $\sqrt{\frac{v}{\lambda_1\delta}} \leq \gamma$ is satisfied and $y\left(t_0\right) \in \mathcal{S}_{\mathcal{D}}$, the assumption that $y\left(t\right) \in \mathcal{D}$, $\forall t \in [t_0,\infty)$ is satisfied. Note that a proper selection of the control gains α, k_1, k_2, β, and Γ, and the selectable constant ε can guarantee that $y\left(t_0\right) \in \mathcal{S}_{\mathcal{D}}$. Furthermore, Equation (4.23) in the theorem statement can be obtained by using (4.19) and (4.28). The result in (4.23) implies that $y \in \mathcal{L}_\infty$, and the definition of y from (4.18) implies that $r, \operatorname{Tanh}\left(e_f\right), \tilde{\theta} \in \mathcal{L}_\infty$. Using the definitions of e in (4.1) and r in (4.2), and considering the fact that x_d is user-defined and is bounded, it can be proven that $e, x \in \mathcal{L}_\infty$. Equations (2.4) and (4.12), and the fact that $\tilde{\theta} \in \mathcal{L}_\infty$, implies that $\hat{\theta} \in \mathcal{L}_\infty$. Using the definition of the parameter estimate law in (4.15) and Assumption 4.1 proves that $\hat{g}_\phi, \hat{g}_\phi^+ \in \mathcal{L}_\infty$. Lastly, since $\dot{x}_d$ is designed to be bounded and all the terms in (4.14) are bounded, u is bounded such that $u \in \mathcal{L}_\infty$. □

4.3 Simulation

A series of numerical simulations were conducted to illustrate the efficacy of the developed saturated ARISE controller and to compare its performance with a standard saturated SM controller. The dynamic model considered during the simulations was similar to a two-state Van der Pol Oscillator; however the dynamic model was modified to be switched and to include disturbances. The modified dynamics also have a control-affine control input. Specifically, the unknown drift dynamics used in the simulations were

$$f_\sigma(x) = \begin{bmatrix} \mu\sigma\left(x_1 - \frac{1}{3}x_1^3 - x_2\right) \\ \frac{1}{\mu\sigma}x_1 \end{bmatrix},$$

where $x = [x_1, x_2]^T$, $\mu \in \mathbb{R}_{>0}$ is an unknown system parameter, and

$$\sigma = \begin{cases} 1, & x_1 \geq 0 \\ 2, & \text{otherwise} \end{cases} \tag{4.29}$$

is an unknown switching signal that depends on the first state and indicates the index of the drift dynamics. The disturbances used during the simulations were $d(t) = [d_1 \cos(t), d_2 \sin(t)]^T$, where $d_1, d_2 \in \mathbb{R}_{>0}$ are unknown constants whose values were varied across simulations based

Table 4.1: Disturbance Sets used in the simulations

Disturbances	d_1	d_2
a	0.01	0.01
b	0.05	0.05
c	0.1	0.1
d	0.5	0.5
e	1	1
f	1.5	1.5

Table 4.2: Simulated control effectiveness matrix sets

Set Names	g_1	g_2	g_3	g_4
GA	12	10	5	2
GB	10	8	3	4
GC	15	6	3	5

on Table 4.1. The control effectiveness matrix used during the simulations was

$$g_\phi\left(x,t\right)=\begin{bmatrix} g_1\phi_1\left(x\right)+g_2\phi_2\left(x\right) & 0 \\ 0 & g_3\phi_1\left(x\right)+g_4\phi_2\left(x\right) \end{bmatrix},$$

where $g_1, g_2, g_3, g_4 \in \mathbb{R}$ are unknown non-zero constants whose values were varied across the simulations based on Table 4.2, and

$$\phi_1\left(x\right)\triangleq\begin{cases} 1, & x_2\geq 0 \\ 0, & \text{otherwise} \end{cases} \quad \textit{and} \tag{4.30}$$

$$\phi_2\left(x\right)\triangleq\left(1-\phi_1\left(x\right)\right) \tag{4.31}$$

are known state-dependent switching signals. The index of the control effectiveness matrix is

$$\phi=\begin{cases} 1, & \phi_1=1 \\ 2, & \phi_1=0 \end{cases},$$

based on the switching signals defined in (4.30) and (4.31). As per the Assumption 2.4, $g_\phi u$ can be linearly parameterized as

$$g_\phi u = \underbrace{\begin{bmatrix} \phi_1 u_1 & (1-\phi_1)\, u_1 & 0 & 0 \\ 0 & 0 & \phi_1 u_2 & (1-\phi_1)\, u_2 \end{bmatrix}}_{Y} \underbrace{\begin{bmatrix} g_1 \\ g_2 \\ g_3 \\ g_4 \end{bmatrix}}_{\theta},$$

where control input $u = [u_1, u_2]^T$.

The desired trajectory for the states used in the simulation was $x_d = [5\cos(t), 5\sin(t)]^T$, and the initial conditions were $x(t_0) = \begin{bmatrix} 3 & 2 \end{bmatrix}^T$. The saturated ARISE controller feedback gains were selected as $k_1 = 2.5$, $k_2 = 115$, $\alpha = 0.5$, $\beta = 85$, and $\Gamma = 0.8 \times \mathrm{diag}\{2, 3, 2, 3\}$. The initial conditions for the parameter approximation were selected as $\hat{\theta}(t_0) = \begin{bmatrix} 2 & 10 & 3 & 5 \end{bmatrix}^T$. A time step of 0.002 seconds was used in the simulation. The performance of the developed saturated ARISE control law was compared with a saturated SM controller across varying dynamic parameters and disturbances to analyze the robustness of both controllers. To do this, the performance of the control laws were compared across 5 different sets of disturbances as presented in Table 4.1. Then, the performance of both controllers were compared across 3 different sets of control effectiveness parameters as presented in Table 4.2. Finally, the performance of the controller was analyzed across varying values of μ evenly spaced from 0.5 to 5. The default values used in the simulations were $\mu = 1.5$, disturbance set $=$ 'd', and control effectiveness set $=$ 'GA'.

The control law used in the simulations for the saturated SM controller for comparison purposes is defined as $u = \hat{g}_\phi^+(x(t), t)(-k_4 \mathrm{sgn}(e) - k_5 \tanh(e(t)) + \dot{x}_d(t))$, where k_4 is a SM control gain and k_5 is a saturated feedback control gain. The values of the control gains used for the SM controller were $k_4 = 2.5$ and $k_5 = 60$. The above mentioned gains for the saturated ARISE and the saturated SM controllers were adjusted using an empirical based method for a single set of dynamic parameters and disturbances (i.e., the default system parameters). The gain selection started with assigning random gains that satisfied the gain conditions in (4.24). These gains were then adjusted iteratively to achieve an improved performance (i.e., minimum tracking errors). First, the gain values for the saturated ARISE controller were determined. After that, the gain values for the standard SM controller were selected. Similar to the saturated ARISE adaptive update law, an adaptive law, defined as $\dot{\hat{\theta}}(t) \triangleq \text{Proj}\left(\Gamma Y_{\phi}^{T}(x(t), t, u(t))\, e(t)\right)$, was developed for the saturated SM controller to estimate the unknown parameters in the control effectiveness matrix. The same initial estimates for θ and adaptive gains Γ were used for both adaptive laws to ensure a fair comparison between the controllers. The RMS trajectory tracking error values were used as a measure to assess the overall performances of both controllers when subjected to varying dynamic parameters and disturbances, allowing for a comprehensive comparison of their effectiveness when employed on a switched system.

4.4 Result/Discussion

The tracking results of the proposed saturated ARISE controller and the saturated SM controller for a single set of dynamic parameters and disturbances are illustrated in Figure 4.1. Referencing Figure 4.1, it can be seen that the tracking errors first converge exponentially and then decrease more slowly with time for both saturated controllers. This is largely due to the fact that the adaptive update laws are improving the adaptive estimates. However, the tracking error performance of the proposed saturated ARISE controller is improved (i.e., smaller errors) compared to the saturated SM controller, proving the effectiveness of the saturated ARISE controller over the saturated SM controller. The decrease in the tracking error values for the ARISE controller is likely due to the ARISE controller implementing an integral SM term instead of a SM term itself. Figure 4.2 shows the RMS errors of the controllers at different disturbance values (refer to Table 4.1). Referencing Figure 4.2, there are negligible differences in the RMS error values for both controllers across varying disturbance

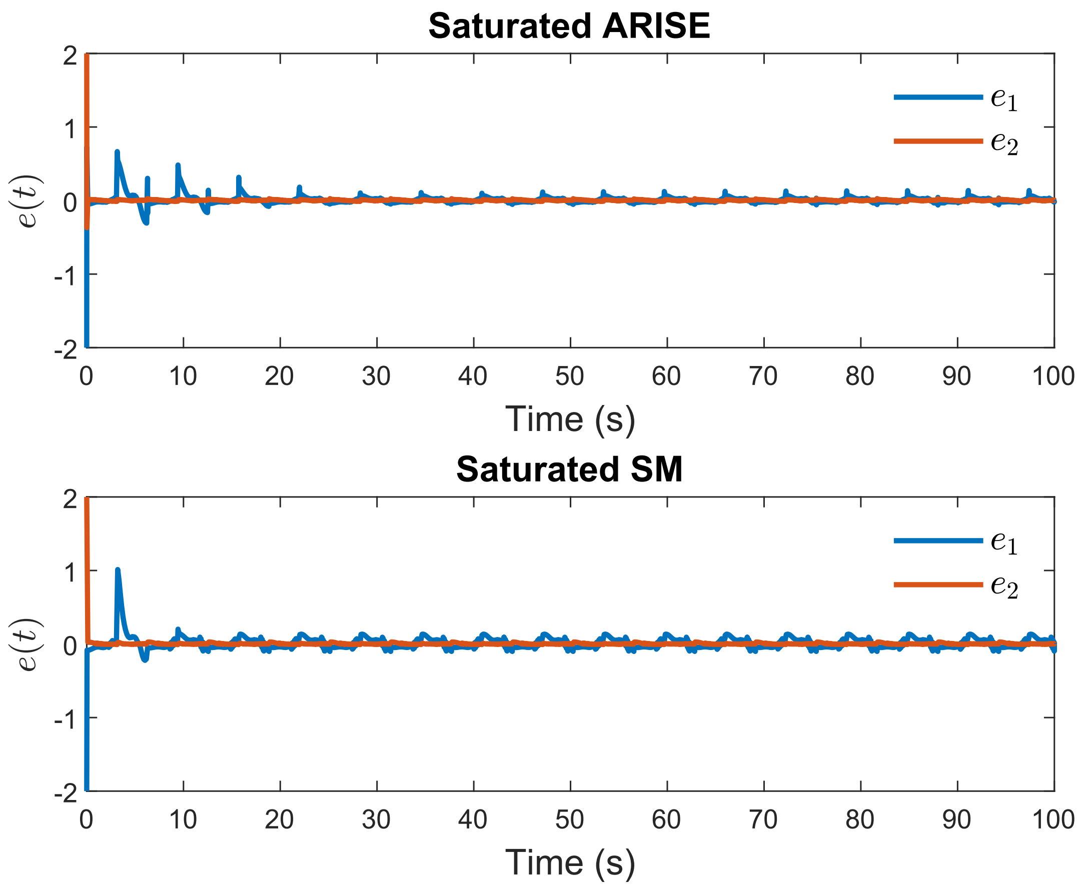

Figure 4.1: Tracking error comparison for the dynamic parameters $\mu = 1.5$, $g_1 = 12$, $g_2 = 10$, $g_3 = 5$, $g_4 = 2$ (i.e., set $'\mathrm{GA}'$), $d_1 = 0.5$, and $d_2 = 0.5$ (i.e., set $'\mathrm{d}'$).

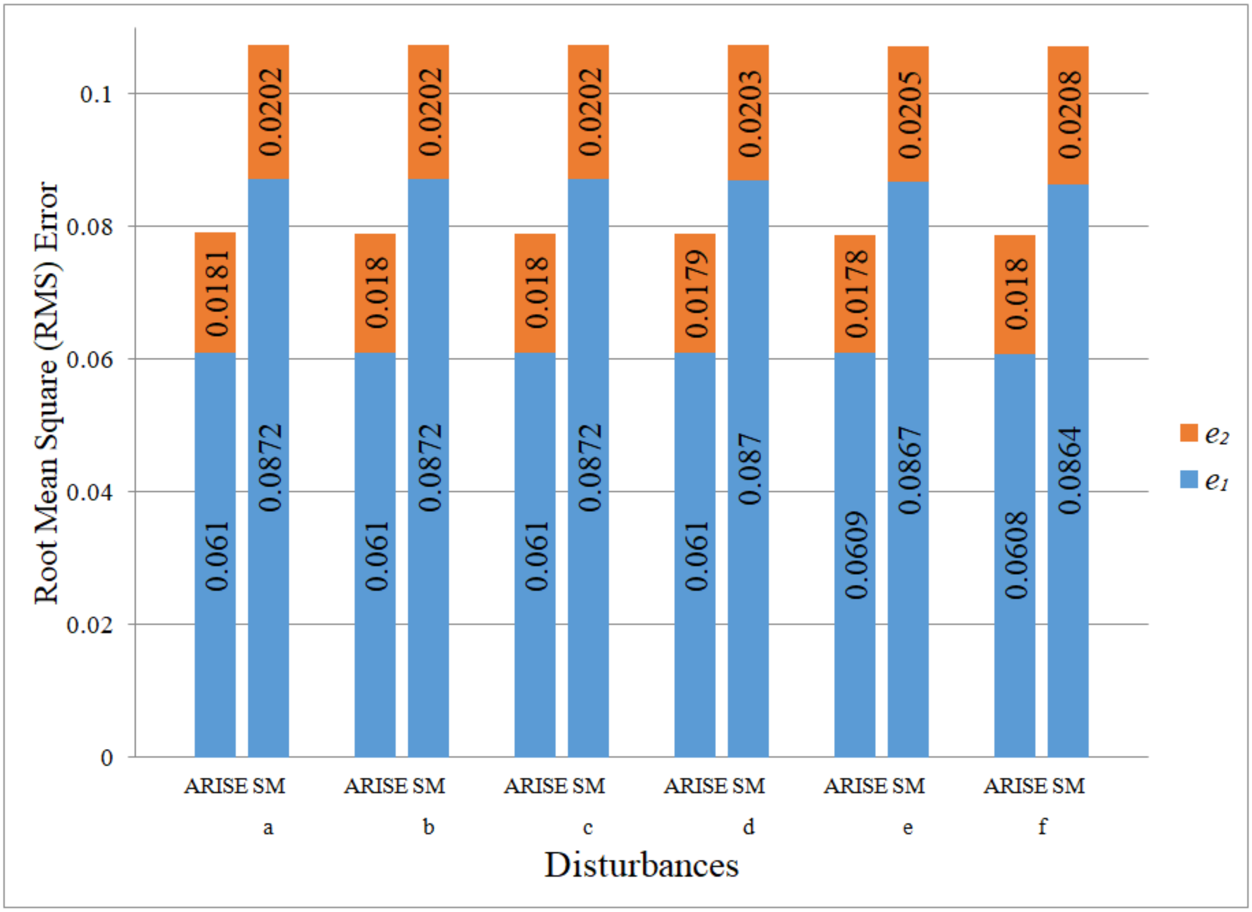

Figure 4.2: RMS tracking errors across varying disturbances when $\mu = 1.5$, $g_1 = 12$, $g_2 = 10$, $g_3 = 5$, and $g_4 = 2$ (i.e., set $'GA'$). The terms $'a'$-$'f'$refer to the disturbances listed in Table 4.1.

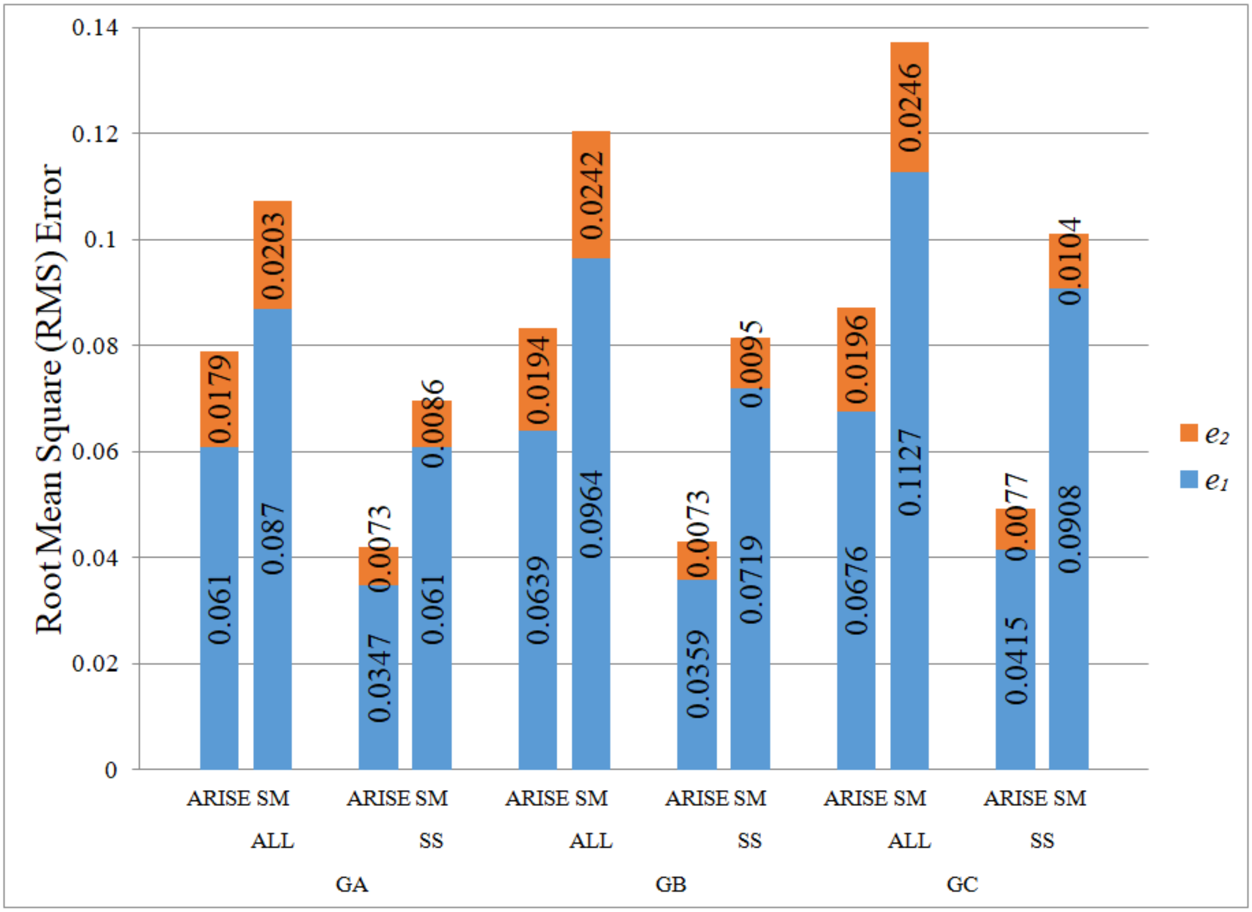

Figure 4.3: RMS tracking errors across varying dynamic parameters when $\mu = 1.5$, $d_1 = 0.5$, and $d_2 = 0.5$ (i.e., set $'\mathrm{d}'$). The RMS errors of the system after steady state (SS) were also evaluated. The states of the system after 10 seconds were considered as SS. The dynamic parameters $'\mathrm{GA}'$, $'\mathrm{GB}'$, and $'\mathrm{GC}'$ refer to the control effectiveness parameters in Table 4.2.

sets, which shows that the controllers are robust to disturbances. It can also be seen from Figure 4.2 that the RMS errors of the saturated ARISE controller are consistently smaller than the saturated SM controller, indicating that the saturated ARISE controller is superior to the saturated SM controller in terms of state tracking performance when controlling a switched system. Additionally, the RMS errors of the proposed saturated ARISE controller and the saturated SM controller are also evaluated at different control effectiveness parameters (refer to Table 4.2) as depicted in Figure 4.3 to analyze their robustness across varying control effectiveness parameters. The RMS error values for both control systems lowered once the systems reached steady state (SS) for each set of control effectiveness parameters.

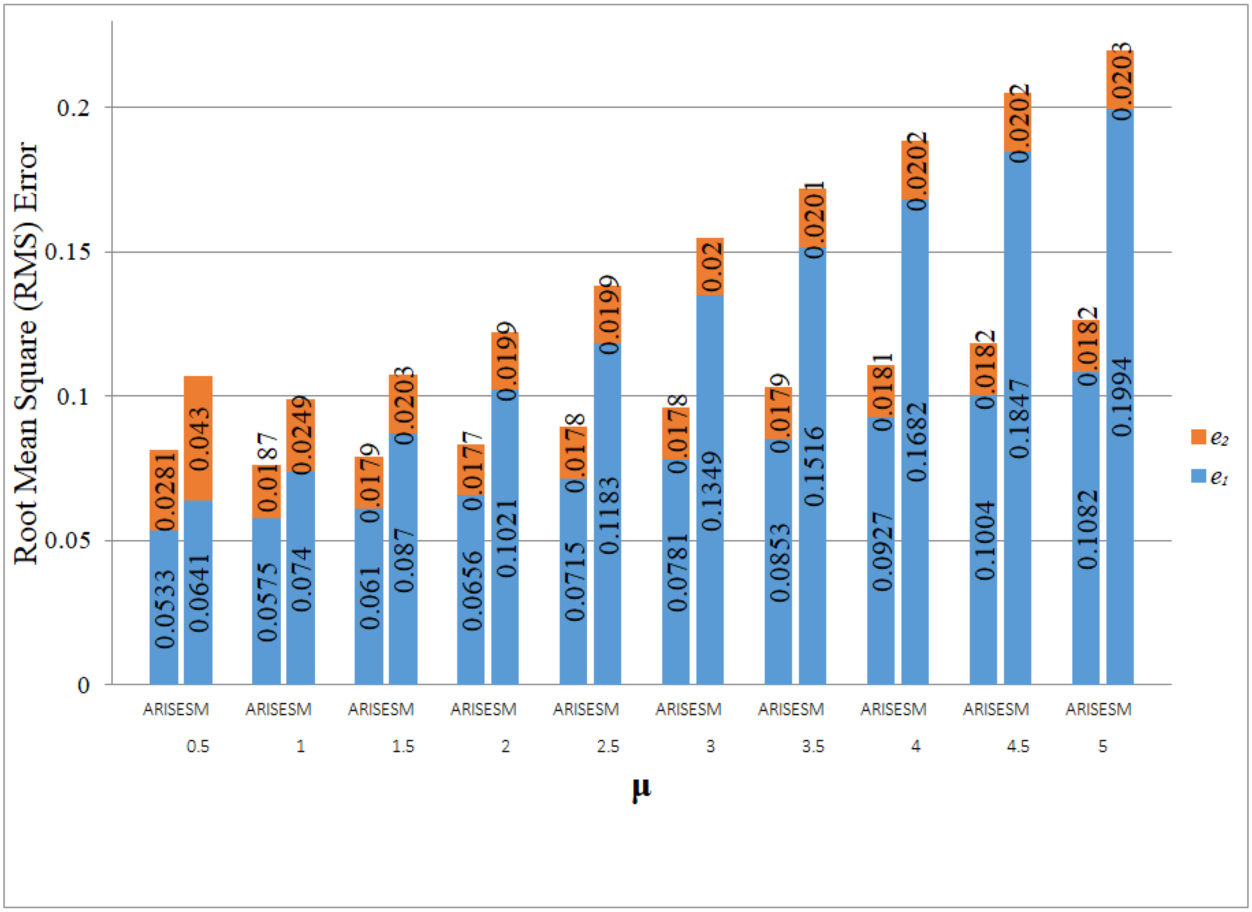

Figure 4.4: RMS tracking errors across varying values of the dynamic parameter μ when $g_1 = 12$, $g_2 = 10$, $g_3 = 5$, $g_4 = 2$ (i.e., set $'$GA$'$), $d_1 = 0.5$, and $d_2 = 0.5$ (i.e., set $'$d$'$).

Similar to prior result, the RMS errors of the saturated ARISE controller were lower for all variations of the control effectiveness parameters compared to the saturated SM controller. Furthermore, Figure 4.4 depicts the RMS tracking errors of the proposed controller and the saturated SM controller across varying values of the dynamic parameter μ. From Figure 4.4, the RMS tracking errors for both controllers increase in magnitude with greater values of μ. However, the RMS errors of the saturated ARISE controller increases at a slower rate with increasing μ and overall are considerably smaller than the saturated SM controller at every dynamic condition, indicating that the saturated ARISE controller is more robust under varying dynamic parameters.

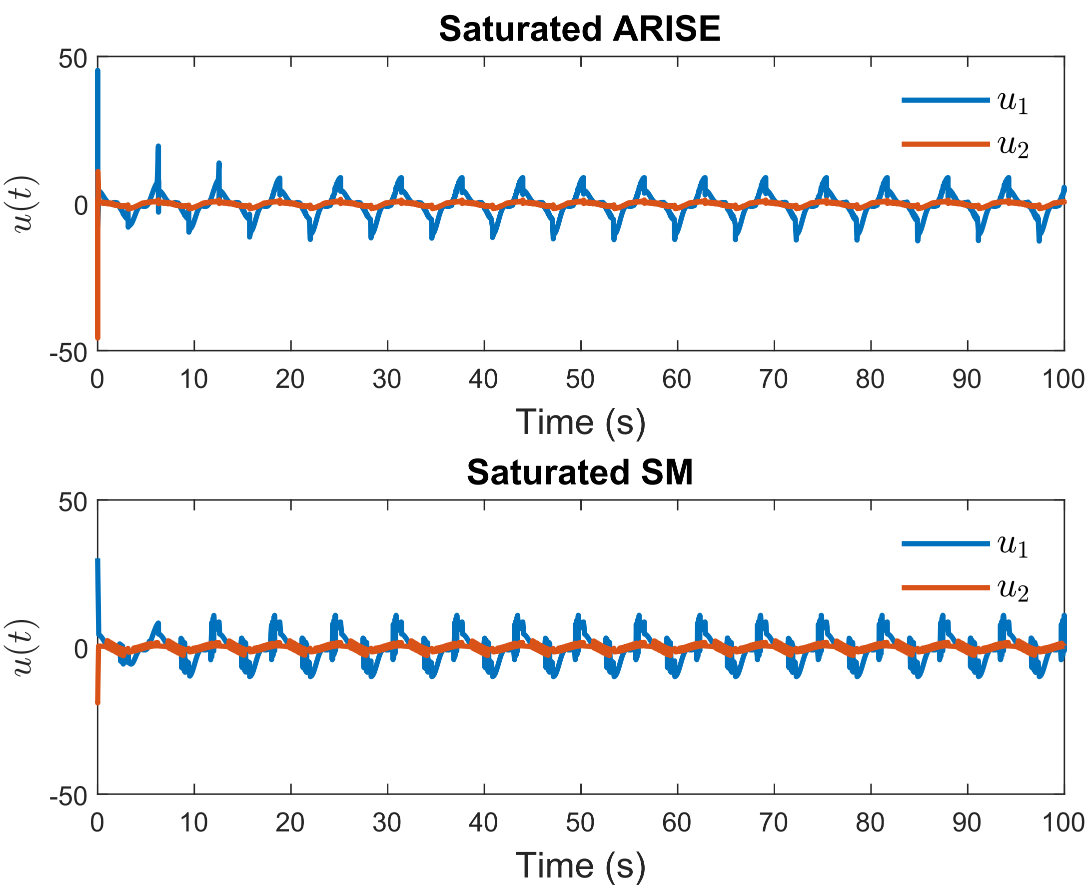

Figure 4.5: Control input comparison when $\mu = 1.5$, $g_1 = 12$, $g_2 = 10$, $g_3 = 5$, $g_4 = 2$ (i.e., set $'\mathrm{GA}'$), $d_1 = 0.5$, and $d_2 = 0.5$ (i.e., set $'\mathrm{d}'$).

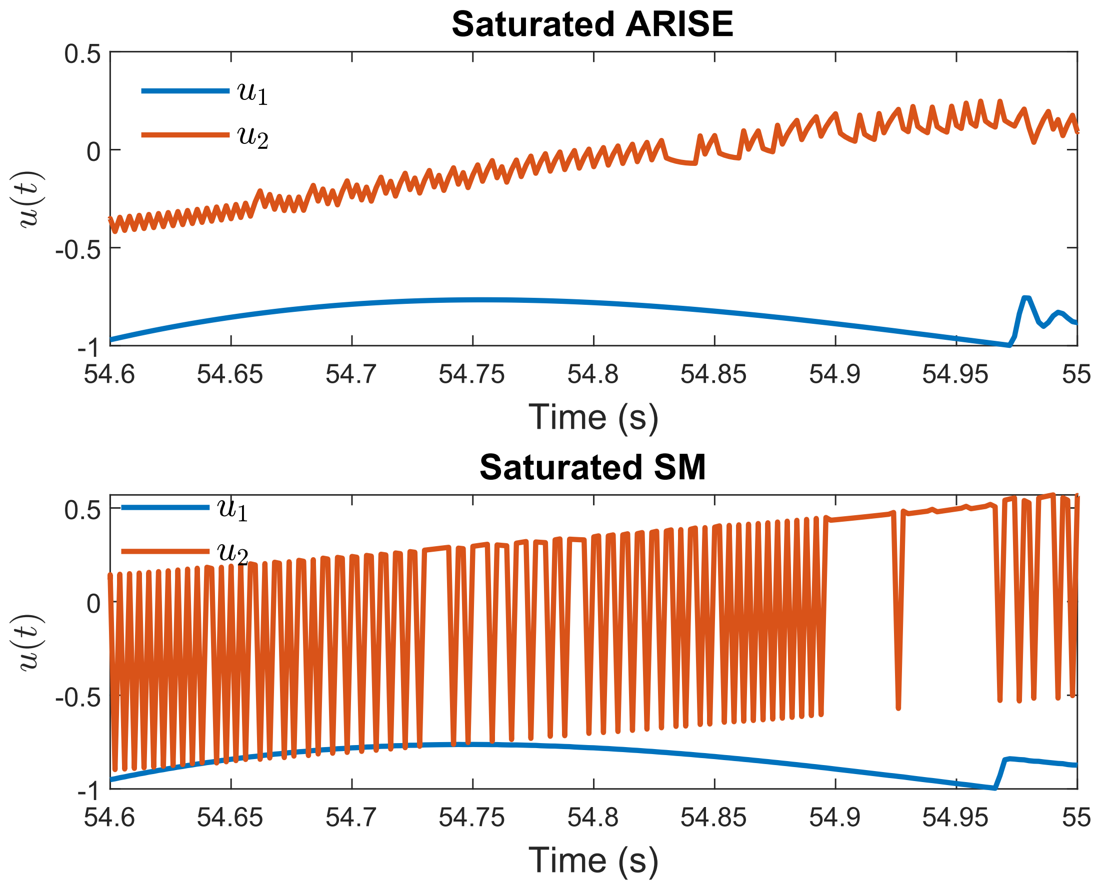

Figure 4.6: Control input comparison depicting the high frequency behavior of SM controllers compared to ARISE controllers when $\mu = 1.5$, $g_1 = 12$, $g_2 = 10$, $g_3 = 5$, $g_4 = 2$ (i.e., set $'$GA$'$), $d_1 = 0.5$, and $d_2 = 0.5$ (i.e., set $'$d$'$).

To further analyze the performance of both controllers, the control inputs required to track the desired trajectory for the switched dynamic system with the default dynamic parameters and disturbances were also determined during the simulations and the results are illustrated in Figure 4.5. Even though the saturated ARISE controller had lower tracking error values, the control effort required to track the given trajectory were similar to the saturated SM controller. Consequently, despite the control inputs being similar, the saturated ARISE controller outperformed the standard saturated SM controller when controlling a switched dynamic system. Figure 4.6 is developed by narrowing the axes in Figure 4.5 to evaluate the control inputs across a narrow subset of time. Referencing Figure 4.6, it is clear that the proposed saturated ARISE controller exhibits smoother control inputs; whereas, the SM controller exhibits rapid switching in the control inputs that is likely to result in chatter during practical implementation. Additionally, designing a saturated control law ensures that the ARISE controller saturates, which ensures the feasibility and applicability of the proposed controller in real-world systems.

4.5 Concluding Remarks

The saturated ARISE controller that accounts for the physical limitations of an actuator was successfully designed in this chapter. An auxiliary error system, similar to that of the previous chapter, was developed; however, the error system designed in Chapter 4 incorporated a smooth hyperbolic tangent function as a saturation function to account for the physical limitations of an actuator. The adaptive law used for the saturated ARISE controller followed from the same development as the ARISE controller. A Lyapunov-like stability analysis ensured that the proposed control law was stable given that the gain conditions and initial conditions were satisfied. The performance of the proposed saturated ARISE controller was compared with a saturated SM controller by evaluating the RMS errors across varying dynamic parameters and disturbances. The simulation results showed that the saturated ARISE controller can outperform the saturated SM controller.

Chapter 5

Conclusion/Future Work

5.1 Conclusion

In Chapter 3 of this thesis, an ARISE control architecture was developed, and the effectiveness of the controller was compared with a traditional general SM controller. The ARISE controller comprises a novel auxiliary error system that is designed to compensate for uncertain terms that are upper bounded by a constant. The chattering effect caused by SM terms is mitigated by the introduction of the novel auxiliary error system. A traditional SM controller has a discontinuous SM term directly in the controller; whereas, the proposed ARISE controller implements an integral of the SM term in the controller. Unlike SM, the integral of a signum function enables a continuous controller, eliminating chattering and the requirement for infinite control frequency. Unlike RISE control, the developed ARISE controller can be applied to switched and nonsmooth systems. The performance of the proposed ARISE controller was evaluated and compared against a traditional SM controller via simulations. Results from the numerical simulations prove that ARISE control can outperform SM control.

In Chapter 4 of this thesis, a saturated ARISE controller that combines adaptive and robust control terms is developed for a nonlinear switched or nonsmooth dynamic system. A Lyapunov-like stability analysis was performed for the proposed control architecture to ensure that the tracking errors remain bounded. A hyperbolic tangent function was incorporated in the control law to create a saturated control input that accounts for the limitations of actuators and ensures reliable, beneficial, and practical performance of the controller when used in real-world physical systems. Another achievement of the proposed controller is its ability to control a switched, uncertain, and nonlinear dynamic system, unlike the standard RISE control approach. The developed control law in this work incorporates an auxiliary error function that produced an excellent tracking performance, surpassing the performance of a standard saturated SM controller, as evidenced by the simulation results. Overall, the proposed saturated controller provided an excellent control performance for a switched, nonsmooth, and nonlinear system.

5.2 Future Work

Future work will investigate mathematical approaches to eliminate the ultimate bound for the ARISE and saturated ARISE controllers. Furthermore, experiments will be performed to experimentally evaluate the performance of the developed ARISE control structures in real systems. Additional simulations will also be performed to compare the effectiveness of the proposed controllers to general RISE controllers while controlling a smooth dynamic system.

References

[1] C. Abdallah, D.M. Dawson, P. Dorato, and M. Jamshidi. Survey of robust control for rigid robots. *IEEE Control System Mag.*, 11(2):24–30, 1991.

[2] H. K. Khalil. *Nonlinear Systems.* Prentice Hall, Upper Saddle River, NJ, 3 edition, 2002.

[3] B. C. Allen, C. Cousin, C. Rouse, and W. E. Dixon. Cadence tracking for switched FES cycling with unknown input delay. In *Proc. IEEE Conf. Decis. Control*, pages 60–65, Nice, Fr, Dec. 2019.

[4] W. E. Dixon, Y. Fang, D. M. Dawson, and J. Chen. Adaptive range identification for exponential visual servo control. In *Proc. IEEE Int. Symp. Intell. Control*, pages 46–51, Houston, Texas, Oct. 2003.

[5] B. Allen, K. Stubbs, and W. E. Dixon. Data-based and opportunistic integral concurrent learning for adaptive trajectory tracking during switched FES-induced biceps curls. *IEEE Trans. Neural Syst. Rehabil. Eng.*, 30:2557–2566, 2022.

[6] V. Duenas, C. A. Cousin, V. Ghanbari, E. J. Fox, and W. E. Dixon. Torque and cadence tracking in functional electrical stimulation induced cycling using passivity-based spatial repetitive learning control. *Automatica*, 115:1–9, 2020.

[7] R. A. Freeman and P. V. Kokotovic. *Robust Nonlinear Control Design: State-Space and Lyapunov Techniques.* Birkhäuser, Boston, MA, 1996.

[8] B. C. Allen, K. J. Stubbs, and W. E. Dixon. Position and cadence tracking of a motorized FES-cycle with an unknown time-varying input delay using saturated FES control. *Automatica*, 139, 2022.

[9] B. C. Allen, K. J. Stubbs, and W. E. Dixon. Robust cadence and power tracking on a switched FES cycle with an unknown electromechanical delay. *IEEE Trans. Control Syst. Tech.*, 31(1):451–458, 2023.

[10] J. Slotine and W. Li. *Applied Nonlinear Control*. Prentice Hall, 1991.

[11] W. E. Dixon, A. Behal, D. M. Dawson, and S. Nagarkatti. *Nonlinear Control of Engineering Systems: A Lyapunov-Based Approach*. Birkhauser: Boston, 2003.

[12] M. J. Bellman, R. J. Downey, A. Parikh, and W. E. Dixon. Automatic control of cycling induced by functional electrical stimulation with electric motor assistance. *IEEE Trans. Autom. Science Eng.*, 14(2):1225–1234, April 2017.

[13] C. M. Kwan, D. M. Dawson, and F. L. Lewis. Robust adaptive control of robots using neural network: Global tracking stability. In *Proc. IEEE Conf. Decis. Control*, pages 1846–1851, New Orleans, Louisiana, 1995.

[14] S. S. Ge, C. C. Hang, and L. C. Woon. Adaptive neural network control of robot manipulators in task space. *IEEE Trans. Ind. Electron.*, 44(6):746–752, 1997.

[15] M.L. Corradini, A. Cristofaro, and G. Orlando. Robust stabilization of multi input plants with saturating actuators. *IEEE Trans. Autom. Control*, 55(2):419–425, 2010.

[16] P. M. Patre, K. Dupree, W. MacKunis, and W. E. Dixon. A new class of modular adaptive controllers, part ii: Neural network extension for non-lp systems. In *Proc. Am. Control Conf.*, pages 1214–1219, Seattle, WA, USA, Jun. 2008.

[17] G. Hu, W. E. Dixon, and H. Ding. Robust tracking control of an array of nanoparticles moving on a substrate. *Automatica*, 48(2):442–448, 2012.

[18] P. M. Patre, W. MacKunis, K. Kaiser, and W. E. Dixon. Asymptotic tracking for uncertain dynamic systems via a multilayer neural network feedforward and RISE feedback control structure. *IEEE Trans. Autom. Control*, 53(9):2180–2185, 2008.

[19] T.-H. Cheng, R. Downey, and W. E. Dixon. Robust output feedback control of uncertain switched euler-lagrange systems. In *Proc. IEEE Conf. Decis. Control*, pages 4668–4673, Florence, IT, Dec. 2013.

[20] W. E. Dixon, D. M. Dawson, E. Zergeroglu, and A. Behal. Adaptive tracking control of a wheeled mobile robot via an uncalibrated camera system. *IEEE Trans. Syst. Man Cybern. Part B Cybern.*, 31:341–352, 2001.

[21] W. E. Dixon, E. Zergeroglu, D. M. Dawson, and M. W. Hannan. Global adaptive partial state feedback tracking control of rigid-link flexible-joint robots. *Robotica*, 18:325–326, 2000.

[22] M. B. Cheng and C. C. Tsai. Hybrid robust tracking control for a mobile manipulator via sliding-mode neural network. In *Proc. IEEE Int. Conf. Mechatron.*, pages 537–542, Taipei, Taiwan, 2005.

[23] C. A. Cousin, C. A. Rouse, V. H. Duenas, and W. E. Dixon. Controlling the cadence and admittance of a functional electrical stimulation cycle. *IEEE Trans. Neural Syst. Rehabil. Eng.*, 27(6):1181–1192, June 2019.

[24] R. Sun, M. Greene, D. Le, Z. Bell, G. Chowdhary, and W. E. Dixon. Lyapunov-based real-time and iterative adjustment of deep neural networks. *IEEE Control Syst. Lett.*, 6:193–198, 2022.

[25] C. Edwards and S.K. Spurgeon. *Sliding Mode Control: Theory And Applications.* Taylor & Francis systems and control book series. Taylor & Francis, 1998.

[26] Hasan Komurcugil, Samet Biricik, Sertac Bayhan, and Zhen Zhang. Sliding mode control: Overview of its applications in power converters. *IEEE Industrial Electronics Magazine*, 15(1):40–49, 2021.

[27] M. Corless and G. Leitmann. Continuous state feedback guaranteeing uniform ultimate boundedness for uncertain dynamic systems. *IEEE Trans. Autom. Control*, 26(5):1139–1144, 1981.

[28] A.S.I. Zinober, O.M.E. Ei-Ghezawi, and S.A. Billings. Multivariable variable-structure adaptive model-following control systems. *IEE Proceedings D (Control Theory and Applications)*, 129:6–12(6), January 1982.

[29] Vadim Utkin and Jason Lee. Chattering problem in sliding mode control systems. pages 346 – 350, 07 2006.

[30] A. Kawamura, H. Itoh, and K. Sakamoto. Chattering reduction of disturbance observer based sliding mode control. *IEEE Transactions on Industry Applications*, 30(2):456–461, 1994.

[31] N. Fischer, Z. Kan, R. Kamalapurkar, and W. E. Dixon. Saturated RISE feedback control for a class of second-order nonlinear systems. *IEEE Trans. Autom. Control*, 59(4):1094–1099, Apr. 2014.

[32] N. Sharma, S. Bhasin, Q. Wang, and W. E. Dixon. RISE-based adaptive control of a control affine uncertain nonlinear system with unknown state delays. *IEEE Trans. Autom. Control*, 57(1):255–259, Jan. 2012.

[33] J. Ting, S. Basyal, and B. C. Allen. Robust control of a nonsmooth or switched control affine uncertain nonlinear system using a novel rise-inspired approach. In *Proc. Am. Control Conf.*, 2023.

[34] P. Patre, S. Bhasin, Z. D. Wilcox, and W. E. Dixon. Composite adaptation for neural network-based controllers. *IEEE Trans. Autom. Control*, 55(4):944–950, 2010.

[35] P. M. Patre, W. MacKunis, K. Dupree, and W. E. Dixon. *RISE-Based Robust and Adaptive Control of Nonlinear Systems*. Birkhauser: Boston, to appear.

[36] P. M. Patre, W. Mackunis, C. Makkar, and W. E. Dixon. Asymptotic tracking for systems with structured and unstructured uncertainties. *IEEE Trans. Control Syst. Technol.*, 16:373–379, 2008.

[37] B. Xian, M. S. de Queiroz, D. M. Dawson, and M. McIntyre. A discontinuous output feedback controller and velocity observer for nonlinear mechanical systems. *Automatica*, 40(4):695–700, 2004.

[38] C. Makkar, G. Hu, W. G. Sawyer, and W. E. Dixon. Lyapunov-based tracking control in the presence of uncertain nonlinear parameterizable friction. *IEEE Trans. Autom. Control*, 52:1988–1994, 2007.

[39] W. E. Dixon, Y. Fang, D. M. Dawson, and T. J. Flynn. Range identification for perspective vision systems. *IEEE Trans. Autom. Control*, 48:2232–2238, 2003.

[40] Zhihua Qu and Jian-Xin Xu. Model-based learning controls and their comparisons using lyapunov direct method. *Asian Journal of Control*, 4(1):99–110, 2002.

[41] Z. Cai, M. S. de Queiroz, and D. M.; Dawson. Robust adaptive asymptotic tracking of nonlinear systems with additive disturbance. *IEEE Trans. Autom. Control*, 51:524–529, 2006.

[42] B. Xian, D. M. Dawson, M. S. de Queiroz, and J. Chen. A continuous asymptotic tracking control strategy for uncertain nonlinear systems. *IEEE Trans. Autom. Control*, 49(7):1206–1211, 2004.

[43] X. Zhang, A. Behal, D. M. Dawson, and B. Xian. Output feedback control for a class of uncertain MIMO nonlinear systems with non-symmetric input gain matrix. In *Proc. IEEE Conf. Decis. Control Eur. Control Conf.*, pages 7762–7767, Seville, Spain, December 2005.

[44] Z. Cai, M. S. de Queiroz, and D. M.; Dawson. Robust adaptive asymptotic tracking of nonlinear systems with additive disturbance. *IEEE Trans. Autom. Control*, 51 no. 3(3):524–529, March 2006.

[45] Bo Zhao, Bin Xian, Yao Zhang, and Xu Zhang. Nonlinear robust adaptive tracking control of a quadrotor uav via immersion and invariance methodology. *IEEE Trans. Ind. Electron.*, 62(5):2891–2902, 2014.

[46] Bin Xian, Marcio S. de Queiroz, and Darren M. Dawson. A continuous control mechanism for uncertain nonlinear systems. In Marcio S. de Queiroz, Michael Malisoff, and Peter Wolenski, editors, *Optimal Control, Stabilization and Nonsmooth Analysis*, pages 251–264. Springer Berlin Heidelberg, Berlin, Heidelberg, 2004.

[47] O. Patil, A. Isaly, B. Xian, and W. E. Dixon. Exponential stability with RISE controllers. *IEEE Control Syst. Lett.*, 6:1592–1597, 2022.

[48] Baris Bidikli, Enver Tatlicioglu, and Erkan Zergeroglu. A robust tracking controller for dynamically positioned surface vessels with added mass. In *Proc. IEEE Conf. Decis. Contr.*, pages 4385–4390, 2014.

[49] Zhikai Yao, Jianyong Yao, and Weichao Sun. Adaptive rise control of hydraulic systems with multilayer neural-networks. *IEEE Trans. Ind. Electron.*, 66(11):8638–8647, 2018.

[50] H. T. Dinh, R. Kamalapurkar, S. Bhasin, and W. E. Dixon. Dynamic neural network-based robust observers for second-order uncertain nonlinear systems. In *Proc. IEEE Conf. Decis. Control*, pages 7543–7548, Orlando, FL, 2011.

[51] S. Bhasin, R. Kamalapurkar, H. T. Dinh, and W.E. Dixon. Robust identification-based state derivative estimation for nonlinear systems. *IEEE Trans. Autom. Control*, 58(1):187–192, Jan. 2013.

[52] S. Obuz, J. R. Klotz, R. Kamalapurkar, and W. E. Dixon. Unknown time-varying input delay compensation for uncertain nonlinear systems. *Automatica*, 76:222–229, February 2017.

[53] Chao Sun, Maojiao Ye, and Guoqiang Hu. Distributed time-varying quadratic optimization for multiple agents under undirected graphs. *IEEE Trans. Autom. Control*, 62(7):3687–3694, 2017.

[54] H. T. Dinh, R. Kamalapurkar, S. Bhasin, and W. E. Dixon. Dynamic neural network-based robust observers for uncertain nonlinear systems. *Neural Netw.*, 60:44–52, Dec. 2014.

[55] P. Patre, W. E. Dixon, K. Kaiser, and W. Mackunis. Asymptotic tracking for uncertain dynamic systems via a multilayer nn feedforward and rise feedback control structure. In *Proc. Am. Control Conf.*, pages 5989–5994, New York, NY, Jul. 2007.

[56] N. Fischer, D. Hughes, P. Walters, E. Schwartz, and W. E. Dixon. Nonlinear RISE-based control of an autonomous underwater vehicle. *IEEE Trans. Robot.*, 30(4):845–852, Aug. 2014.

[57] Z. Cai, M. S. de Queiroz, and D. M. Dawson. A sufficiently smooth projection operator. *IEEE Trans. Autom. Control*, 51(1):135–139, January 2006.

[58] A. F. Filippov. Differential equations with discontinuous right-hand side. In *Fifteen papers on differential equations*, volume 42 of *American Mathematical Society Translations - Series 2*, pages 199–231. American Mathematical Society, 1964.

[59] B. E. Paden and S. S. Sastry. A calculus for computing Filippov's differential inclusion with application to the variable structure control of robot manipulators. *IEEE Trans. Circuits Syst.*, 34(1):73–82, January 1987.

[60] E. Aguinaga-Ruiz, A. Zavala-Rio, V. Santibanez, and F. Reyes. Global trajectory tracking through static feedback for robot manipulators with bounded inputs. *IEEE Trans. Control Syst. Technol.*, 17(4):934–944, July 2009.

[61] A. Zavala-Rio and V. Santibanez. A natural saturating extension of the PD-with-desired-gravity-compensation control law for robot manipulators with bounded inputs. *IEEE Trans. Robot.*, 23(2):386–391, 2007.

[62] V. Santibanez, R. Kelly, and M. Llama. A novel global asymptotic stable set-point fuzzy controller with bounded torques for robot manipulators. *IEEE Trans. Fuzzy Syst.*, 13(3):362–372, 2005.

[63] Yuxin Su, P.C. Muller, and Chunhong Zheng. Global asymptotic saturated PID control for robot manipulators. *IEEE Trans. Control Syst. Technol.*, 18(6):1280–1288, November 2010.

[64] S. Basyal, J. Ting, and B. C. Allen. Rise-like saturated control for nonsmooth and switched nonlinear systems. In *ASME Int. Mech. Eng. Congr. Expo. (IMECE)*, 2023.